Study of the Structure of Perfluoro Ethers: Structural Models for Poly(perfluoroformaldehyde), Poly(perfluoroethylene oxide), and Poly(perfluoropropylene oxide)

J. Pacansky,* M. Miller, W. Hatton, B. Liu, and A. Scheiner

Contribution from the IBM Almaden Research Center, 650 Harry Road, San Jose, California 95120-6099. *Received October 10, 1989*

Abstract: Molecular structures have been determined for perfluorodimethyl ether, perfluorodiethyl ether, perfluoromethyl perfluoroethyl ether, and model compounds for polyperfluorinated ethers. Optimized geometries, net charges, molecular orbital energies and plots, bond stretching force constants, vibrational frequencies, and infrared intensities are reported with use of ab initio SCF calculations. In addition, experimental infrared spectra of perfluorinated ethers in argon matrixes and as neat films are compared with theoretical spectra. The data presented herein provide an excellent basis for understanding the structure of the ethers and assigning the infrared band centers. In addition, molecular mechanics is used to obtain insight for the catalytic behavior of the polymeric materials on metal oxide surfaces.

Introduction

Poly(perfluoro ethers) are viscous liquids with exceptional chemical and physical properties which are used extensively in industry as lubricants,[1] dielectric fluids,[2,3] diffusion pump oils,[4-6] and due to their high O_2 solubility[7,8] blood substitutes.[9] The poly(perfluoro ethers) that are used extensively are prepared by direct fluorination of polyethers,[10] by photooxidation of perfluoroethylene[11] and perfluoropropylene,[12] or by direct electrochemical fluorination.[13]

Several materials are commonly manufactured and, hence, are widely used; the theme of this report is centered about these perfluorinated ethers. The possible structures for the polymeric materials produced during the photooxidation process are poly(perfluoroformaldehyde) [PPFF, $-(CF_2-O-)_x$], poly(perfluoroethylene oxide) [PPFEO, $-(CF_2CF_2-O-)_x$], poly(perfluoropropylene oxide) [PPFPO, $-(CF(CF_3)CF_2-O-)_x$], and the copolymers poly(perfluoroformaldehyde-*co*-perfluoroethylene oxide) [PPFFPFEO, $-(CF_2-O-)_x-(CF_2CF_2-O-)_y$] and poly(perfluoroformaldehyde-*co*-perfluoropropylene oxide) [PPFFPFPO, $-(CF_2-O-)_x-(CF(CF_3)CF_2-O-)_y$]. The homopolymer PPFPO and the copolymers PPFFPFEO and PPFFPFPO are commercially available; however, the homopolymers PPFF and PPFEO do not appear to be commercially available.

Due to the widespread use of poly(perfluoro ethers), the mechanisms for thermal degradation have been investigated. Sianesi et al.[1] have studied the thermal degradation of PPFPO at high temperatures and noted that decomposition of the polymer commenced at 350 °C under inert conditions and at 300 °C in the presence of metals. The stable products ultimately formed are C_3F_6, CF_3COF, and COF_2; the latter two hydrolyze to HF, CF_3COOH, and $HF + CO_2$, respectively. The major product is COF_2 when the decomposition is performed in an oxygen atmosphere. Eyring and co-workers[14] studied the thermal decomposition of PPFPO on Ti surfaces using reflectance spectroscopy to follow the reaction; a decrease in reflectance occurred when Ti was converted to TiF_3 by the thermal decomposition products of PPFPO. They concluded that the rate of Ti corrosion is enhanced by the presence of O_2, and there also is a direct dependence of the rate of corrosion on the amount of TiF_3 initially on the titanium surface.

In essence most of the available work on the thermal decomposition of PPFEO and PPFPO deals with final product distributions, and hence does not directly address the mechanistic details required to understand the polymer degradation. Sianesi and co-workers,[1] however, speculate that the degradation is of the free radical type; the initiation reaction, a C-C rupture, is followed by a series of β-scission reactions to decompose large segments of the macromolecule with the evolution of gaseous molecules.

A reasonable point at which to start any investigation into the chemical and physical properties of a material is at the molecular level, more specifically, the molecular structure, chemical bonding, and spectroscopic properties of the ground electronic state, because it is this state that dictates chemistry and physical properties. In this report, we present theoretical and experimental results on perfluorinated ethers. Initially, studies are shown on simple ethers like $(CF_3)_2O$, $(CF_3CF_2)_2O$, and $CF_3OCF_2CF_3$. The geometries are optimized and vibrational frequencies and infrared intensities are computed; these are subsequently compared with available experimental values and new data given herein. Model compounds for PPFF, PPFEO, and PPFPO are presented which are designed to closely mimic a monomeric unit in the homopolymers. Optimized geometries and vibrational frequencies are also computed for the model compounds and also compared with experimental infrared spectra to offer an assignment for the complicated polymeric materials.

Experimental Section

Materials. Perfluorodiethyl ether, $CF_3CF_2-O-CF_2CF_3$, was purchased from Strem Chemicals Inc., Newburyport, MA, with a stated purity of 90%. The purity was further investigated by performing tandem gas chromatography-infrared analysis. The volatile perfluorinated sample was only poorly retained by the GC column: in spite of this, we did determine that the sample consisted of two components: the major com-

(1) Sianesi, D.; Zamboni, V.; Fontanelli, R.; Binaghi, M. *Wear* **1971**, *18*, 85.
(2) Devins, J. C. *Natl. Acad. Sci. NRC Annu. Rep.* **1977**, 398.
(3) Luches, A.; Provenzano, I. *J. Phys. D: Appl. Phys.* **1977**, *10*, 339.
(4) Holland, L.; Laurenson, L.; Baker, P. N. *Vacuum* **1972**, *22*, 315.
(5) Hennings, J.; Lotz, H. *Vacuum* **1977**, *27*, 171.
(6) Laurenson, L.; Dennis, N. T. M.; Newton, J. *Vacuum* **1979**, *29*, 433.
(7) Lawson, D. D.; Moacanin, J.; Scherer, K. V., Jr.; Terranova, T. F.; Ingham, J. D. *J. Fluorine Chem.* **1978**, *12*, 221.
(8) Wessler, E. P.; Iltis, R.; Clark, L. C., Jr. *J. Fluorine Chem.* **1977**, *9*, 137.
(9) Artificial Blood *Fed. Proc.* **1975**, *34*, 1428. Inert Organic Liquids for Biological Oxygen Transport *Fed. Proc.* **1970**, *29*, 1695. Geyer, R. P. In *Drug Design*; Ariens, E. J., Ed.; Academic Press: New York, 1976; Vol. VIII, p 1.
(10) Gerhardt, G. E.; Lagow, R. L. *J. Chem. Soc., Chem. Commun.* **1977**, 259.
(11) Warnell, J. L. US Patent 3,125,599 (March 17, 1964). Barnaba, P.; Cordishi, D.; Lenzi, M.; Mele, A. *Chim. Ind. (Milan)* **1966**, *47*, 1060. Donato, A.; Lenzi, M.; Mele, A. *J. Macromol. Sci. (Chem.)* **1967**, *A1*, 429.
(12) Sianesi, D.; Pasetti, A.; Corti, C. *Makromol. Chem.* **1965**, *86*, 308. Sianesi, D.; Fontanelli, R. *Makromol. Chem.* **1967**, *102*, 115.
(13) Simmons, J. H. U.S. Patent 2,519,983 (1950). Simons, J. H. In *Encyclopedia of Electrochemistry*; Hampel, C. A., Ed.; Reinhold: New York; Chapman and Hall: London, 1964.
(14) Chandler, W. L.; Lloyd, L. B.; Farrow, M. F.; Burnham, R. K.; Eyring, E. M. *Corrosion* **1980**, *36*, 152.

0002-7863/91/1513-329$02.50/0

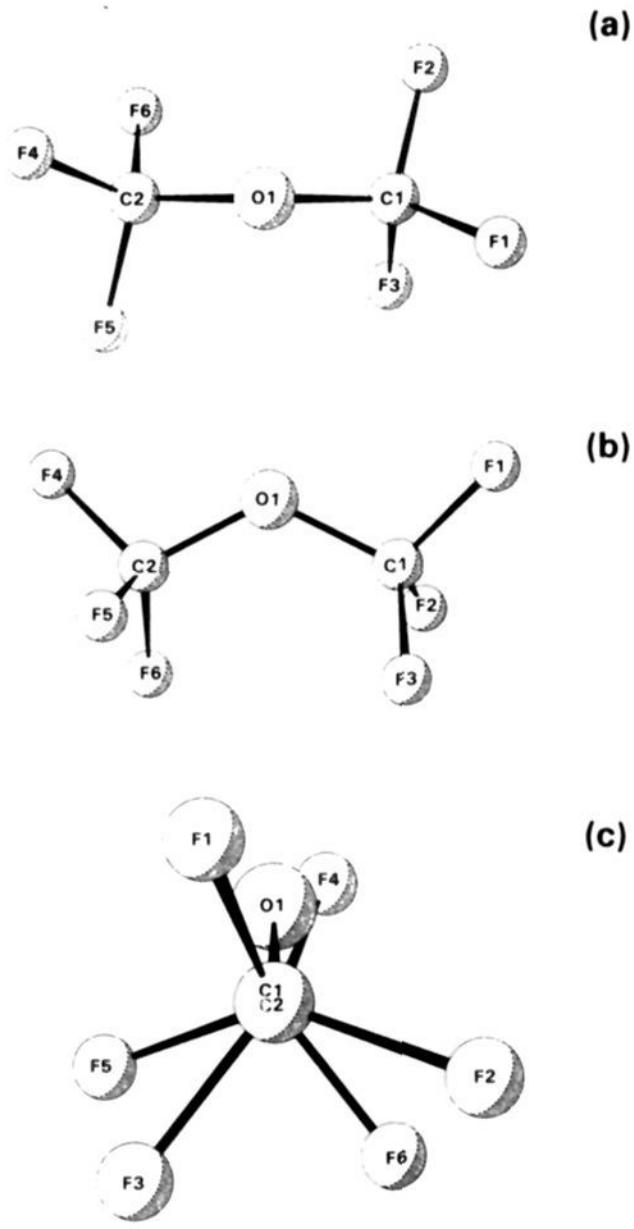

Figure 1. A computer drawing for the optimized geometry of perfluorodimethyl ether.

Table I. The Optimized Bond Lengths (Å) for Perfluorodimethyl Ether Obtained with the STO-3G, 3-21G, 4-31G, and 6-31G* Basis Sets[a]

bond	STO-3G	3-21G	4-31G	6-31G*	exptl
C1–O1	1.431	1.370	1.369	1.356	1.369 (4)
O1–C2	1.431	1.370	1.369	1.356	1.369 (4)
C1–F1	1.363	1.322	1.331	1.301	1.327 (2)
C1–F2	1.367	1.331	1.342	1.308	1.327 (2)
C1–F3	1.368	1.337	1.347	1.310	1.327 (2)
C2–F4	1.363	1.322	1.331	1.301	1.327 (2)
C2–F5	1.367	1.331	1.342	1.308	1.327 (2)
C2–F6	1.368	1.337	1.347	1.310	1.327 (2)

[a] The experimental values are also included (uncertainties in parentheses).

Table II. The Optimized Bond Angles (deg) for Perfluorodimethyl Ether Obtained with the STO-3G, 3-21G, 4-31G, and 6-31G* Basis Sets[a]

angle	STO-3G	3-21G	4-31G	6-31G*	exptl
C1–O1–C2	113.2	124.1	125.9	121.3	119.1 (8)
F1–C1–F2	109.3	109.3	109.2	109.0	
F1–C1–F3	109.7	109.6	109.6	109.4	
F2–C1–F3	108.8	108.4	108.0	108.3	
F4–C2–F5	109.3	109.3	109.2	109.0	
F4–C2–F6	109.7	109.6	109.6	109.4	
F5–C2–F6	108.8	108.4	108.0	108.3	
F1–C1–O1	106.7	107.9	107.6	107.1	
F2–C1–O1	110.9	111.1	111.1	111.3	
F3–C1–O1	111.3	110.5	111.3	111.9	
F4–C2–O1	106.7	107.9	107.6	107.1	
F5–C2–O1	110.9	111.1	111.1	111.3	
F6–C2–O1	111.3	110.5	111.3	111.9	
⟨F1C1O1⟩ ⟨C1O1C2⟩	17.8	23.4	18.0	16.8	
⟨F4C2O1⟩ ⟨C2O1C1⟩	17.8	23.4	18.0	16.8	

[a] The experimental values are also included (uncertainties in parentheses).

ponent was perfluorodiethyl ether, and the other, present in a much lower concentration, is a fluorine-containing material with physical properties and an infrared spectrum very similar to those for perfluorodiethyl ether. The infrared absorptions attributed to the impurity are marked by an asterisk in the figures where appropriate.

The perfluoro ether CF_3CF_2O–$((CF_3)CFCF_2O$–$)_4CF_2CF_3$, a propylene oxide oligomer, hereafter referred to as the PPFPO tetramer, was obtained from Dr. J. D. Patton, E. I. DuPont De Nemours & Co., Wilmington, DE. The sample consisted of 95% of the perfluorinated structures; the major part of the 5% impurities was made up of two materials with slightly different end groups: the first impurity has a methylene fluorine replaced by a hydrogen on the terminal ethyl group

$$CF_3CF_2O\text{–}((CF_3)CFCF_2O\text{–})_4CFHCF_3$$

and the second impurity has a perfluoroisopropyl group capping the chain rather than a perfluoroethyl group

$$CF_3CF_2O\text{–}((CF_3)CFCF_2O\text{–})_4CF(CF_3)CF_3$$

Due to the large number of oscillators per chain, a long path length would have to be used to detect the vibrations associated with the single CH and the isopropyl group even if we examined oligomers terminated only by $-CFHCF_3$ and $-CF(CF_3)CF_3$ groups. In view of the fact that 95% of the materials examined in this report were capped with perfluoroethyl groups we do not view the impurities as an issue with our analysis. In spite of this we examined very thick films for absorptions in the CH stretching region; these efforts were not successful.

The homopolymer PPFPO (trademark, Krytox) was obtained from E. I. DuPont De Nemours & Co., Wilmington, DE. The liquid material had a viscosity (η) of 3440 cps and a number average molecular weight (M_n) of 8513. The chemical formula is

$$\text{–}(CF(CF_3)CF_2\text{–}O\text{–})_{40}$$

The copolymers PPFFPFEO and PPFFPFPO were obtained from Montedison USA Inc. and are sold under the trademark Fomblin Fluids. The PPFFPFPO sample (Fomblin YR) had a number average molecular weight (M_n) of 6237[15] and the following structure.

$$\text{–}(CF_2\text{–}O\text{–})_n\text{–}(CF(CF_3)CF_2\text{–}O\text{–})_{20n}$$

The PPFFPFEO sample (Fomblin Z) had M_n = 7176 and the approximate structure shown below:

$$\text{–}(CF_2\text{–}O\text{–})_{35}\text{–}(CF_2CF_2\text{–}O\text{–})_{60}$$

Equipment. The matrix-isolation equipment[16] for the infrared spectroscopy consisted of a gas-handling system, a cryogenic system, and an infrared spectrometer. The gas-handling system was constructed of glass; a Wallace and Tiernan differential pressure manometer was used to monitor the deposition of the rare gas–perfluoro ether mixture through a Granville Phillips variable leak valve. The cryogenic system consisted of an Air products closed cycle refrigerator fitted with CsI substrates and windows. A stainless steel high vacuum system was used to evacuate the gas-handling system and the refrigerator. The vacuum system was pumped by an oil diffusion pump in conjunction with a liquid nitrogen trap. A Perkin-Elmer 580B infrared spectrometer equipped with a 3700 data work station was used to record the spectra.

Sample Preparation. The gaseous ether CF_3CF_2–O–CF_2CF_3 was mixed with argon (Linde Research Purity) to achieve a guest/host ratio of 1/10000; 51 mm of this mixture was deposited from a 3-L reservoir with the CsI substrate at 30 K, and then the CsI substrate was cooled to 10 K to obtain the final sample for spectroscopic analysis.

The vapor pressure of the tetramer was too low to be detected on the differential pressure manometer; we estimate the vapor pressure to be $\simeq$0.01 mm. The gas-handling system was saturated with the vapor pressure of the tetramer and argon (Linde Research Purity) was added to the system to achieve an estimated guest/host ratio of $\simeq$1/1000; this mixture was deposited with the CsI substrate at 20 K to obtain the final sample for spectroscopic analysis. Another tetramer sample was prepared for matrix isolation analysis but at a higher dilution (estimated concentration 1/10000).

The poly(perfluoro ethers) were prepared for spectroscopic analysis by spin coating the materials on CsI substrates to the desired film

(15) Pacansky, J.; Waltman, R. J.; Maier, M. *J. Phys. Chem.* **1987**, *91*, 1225.

(16) Pacansky, J.; Horne, D. E.; Gardini, G. P.; Bargon, J. *J. Phys. Chem.* **1977**, *81*, 2149.

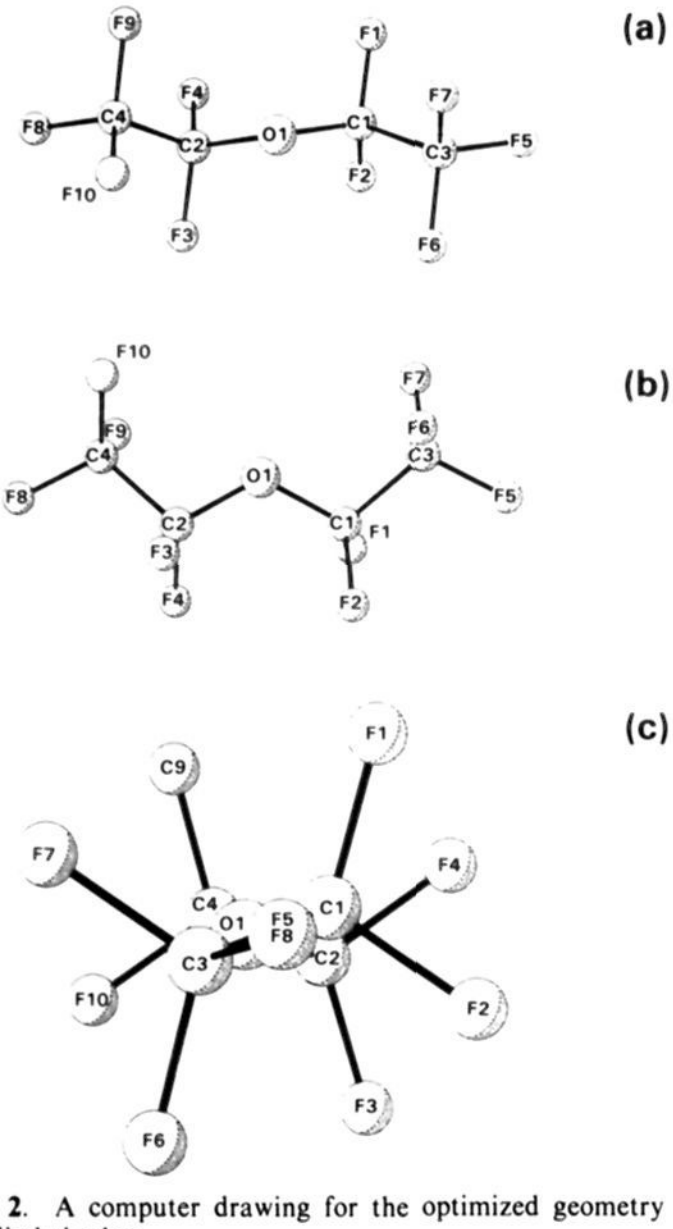

Figure 2. A computer drawing for the optimized geometry of perfluorodiethyl ether.

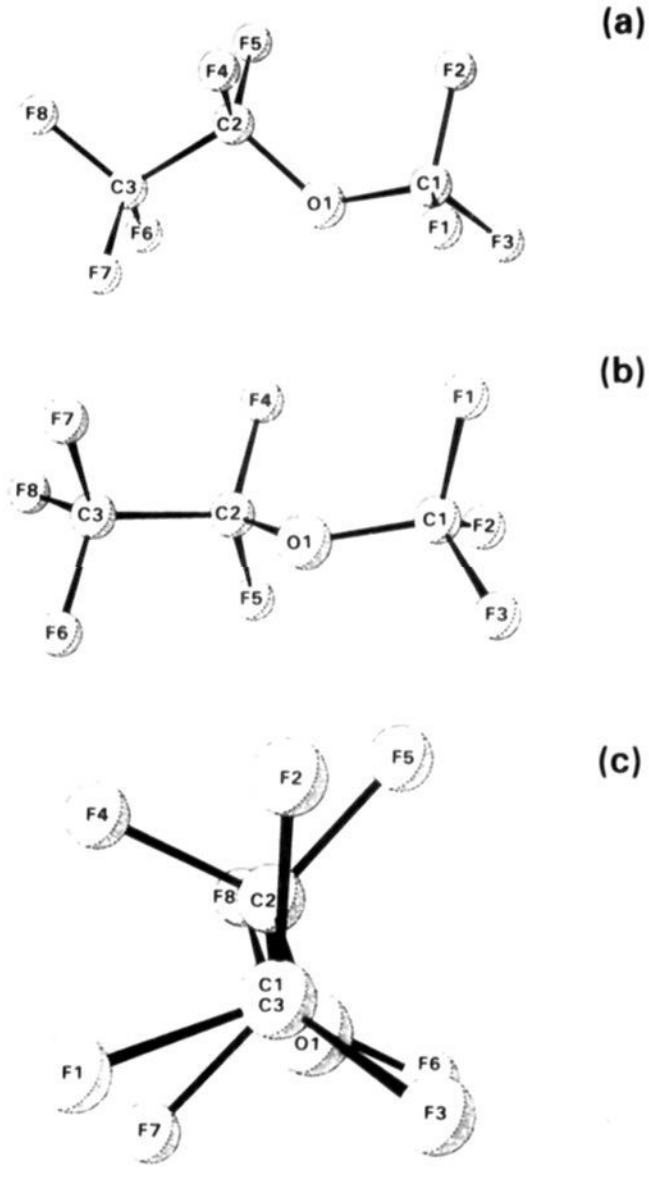

Figure 3. A computer drawing for the optimized geometry of perfluoromethyl perfluoroethyl ether.

Table III. The Optimized Bond Lengths (Å) for Perfluorodiethyl Ether Obtained with the 3-21G Basis Set

bond	3-21G	bond	3-21G	bond	3-21G
C1–O1	1.378	C1–F2	1.349	C3–F6	1.337
O1–C2	1.378	C2–F3	1.344	C3–F7	1.336
C1–C3	1.506	C2–F4	1.349	C4–F8	1.340
C2–C4	1.506	C3–F5	1.340	C4–F9	1.337
C1–F1	1.344			C4–F10	1.336

Table IV. The Optimized Bond Angles (deg) for Perfluorodiethyl Ether Obtained with the 3-21G Basis Set

angle	3-21G	angle	3-21G
C1–O1–C2	123.3	F8–C4–F10	109.2
C3–C1–O1	107.0	F9–C4–F10	109.5
C4–C2–O1	107.0	F1–C1–O1	111.1
C3–C1–F1	110.0	F2–C1–O1	110.5
C3–C1–F2	109.9	F3–C2–O1	111.1
F1–C1–F2	108.4	F4–C2–O1	110.5
C4–C2–F3	110.0	F5–C3–C1	109.5
C4–C2–F4	109.9	F6–C3–C1	109.7
F3–C2–F4	108.4	F7–C3–C1	110.0
F5–C3–F6	109.1	F8–C4–C2	109.5
F5–C3–F7	109.2	F9–C4–C2	109.7
F6–C3–F7	109.5	F10–C4–C2	110.0
F8–C4–F9	109.1	⟨C3–C1–O1⟩ ⟨C1–O1–C2⟩	22.8
		⟨C4–C2–O1⟩ ⟨C2–O1–C1⟩	22.8

thickness. The coated substrates were then mounted into the sample mounts of the low-temperature refrigerators which were then pumped and cooled to $T = 10$ K at which point infrared spectra were recorded.

Computational Details

Ab initio calculations were performed with the vectorized IBM version of the Gaussian 86 program.[17] Geometry optimizations were performed at the SCF level of theory by utilizing the computationally efficient

Table V. The Optimized Bond Lengths (Å) for Perfluoromethyl Perfluoroethyl Ether Obtained with the 3-21G Basis Set

bond	3-21G	bond	3-21G	bond	3-21G
C1–O1	1.373	C1–F2	1.337	C2–F5	1.345
O1–C2	1.375	C1–F3	1.323	C3–F6	1.336
C2–C3	1.505	C2–F4	1.349	C3–F7	1.336
C1–F1	1.330			C3–F8	1.340

Table VI. The Optimized Bond Angles (deg) for Perfluoromethyl Perfluoroethyl Ether Obtained with the 3-21G Basis Set

angle	3-21G	angle	3-21G
C1–O1–C2	124.0	F3–C1–O1	108.2
O1–C2–C3	106.8	F4–C2–O1	110.7
F1–C1–F2	108.6	F5–C2–O1	111.4
F1–C1–F3	110.7	F4–C2–O3	109.8
F2–C1–F3	109.6	F5–C2–C3	109.8
F4–C2–F5	108.3	F6–C3–C2	110.0
F6–C3–F7	109.5	F7–C3–C2	109.8
F6–C3–F8	109.1	F8–C3–C2	109.4
F7–C3–F8	109.0	⟨F3–C1–O1⟩ ⟨C1–O1–C2⟩	32.4
F1–C1–O1	110.7	⟨C3–C2–O1⟩ ⟨C2–O1–C1⟩	15.4
F2–C1–O1	110.4		

3-21G and 4-31G basis sets.[18] In addition, a geometry optimization starting from the RHF/3-21G geometry was performed with use of the medium sized 6-31G* basis set (which contains a single set of d-functions on all atoms). In each case Cartesian force constants, harmonic vibra-

(17) Gaussian 86: M. J. Frisch, J. S. Binkley, H. B. Schlegel, K. Raghavachari, C. F. Melius, R. L. Martin, J. J. P. Stewart, F. W. Bobrowicz, C. M. Rohlfing, L. R. Kahn, D. J. DeFrees, R. Seeger, R. A. Whiteside, D. J. Fox, E. M. Fluder, and J. A. Pople, Carnegie-Mellon Quantum Chemistry Publishing Unit: Pittsburgh, PA, 1984.

(18) For a description of the basis set and MP2, see: Hehre, W.; Radom, L.; Schleyer, P. v. R.; Pople, J. A. *Ab initio Molecular Orbital Theory*, Wiley Interscience: New York, 1986; Chapter 4.

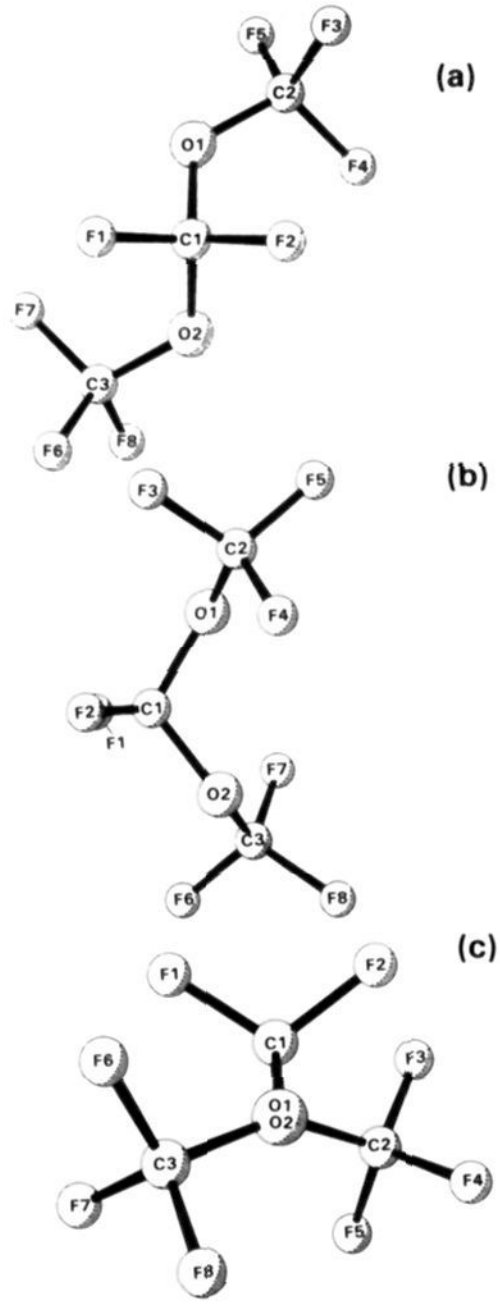

Figure 4. A computer drawing for the optimized geometry of the PPFF model compound.

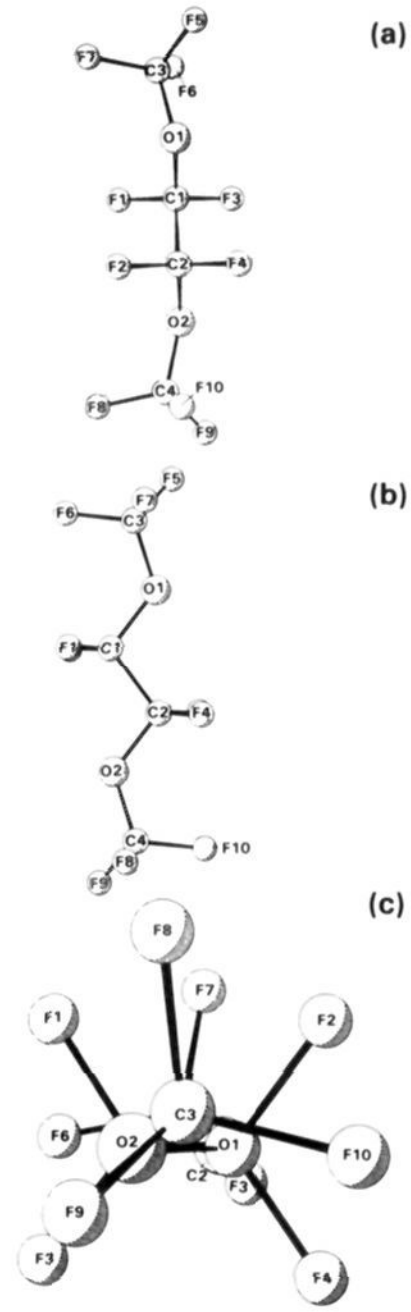

Figure 5. A computer drawing for the optimized geometry of the PPFEO model compound.

tional frequencies, and infrared and Raman intensities were determined by analytic differentiation of the Hartree–Fock wave function. Atomic charges were determined from a standard Mulliken population analysis. All calculations were performed on an IBM 3090 Model 300E at the IBM Almaden Research Center. The RHF/6-31G* force constant–frequency calculation for $(CF_3)_2O$ required approximately 365 min of CPU.

The simplest perfluoro ether $(CF_3)_2O$ is initially considered in detail because the salient features of its structure are also found in more complicated systems. Optimized geometries, vibrational frequencies and infrared intensities were computed with use of the 3-21G, 4-31G, and 6-31G* basis sets. A major result of the basis set studies on $(CF_3)_2O$ was that the 3-21G basis set was a good compromise between dependable results and computer time; consequently, this basis set was used for the larger ethers.

Results and Discussion

The parent perfluoro ether $(CF_3)_2O$ has been structurally examined with use of a number of techniques. The system is of course the prototype for the perfluoro ethers and as a consequence we have theoretically studied it in detail. The results discussed below show that a 3-21G basis may be used to obtain significant results and that most of all the geometry of $(CF_3)_2O$ contains important features that are indeed carried over to the larger ethers.

The results of a microwave spectroscopic study indicated that the C–O–C bond angle in $(CF_3)_2O$ was bent, and hence the molecule may have a C_{2v} symmetry. Bürger and Pawelke[19] performed a normal coordinate analysis and molecular mechanics calculations on the system to investigate whether a C_{2v} with C–F bonds in the C–O–C plane or a C_2 symmetry with C–F bonds twisted out of the C–O–C plane provided a better fit to experimental data. Their results suggested that the C_2 symmetry corresponded to a minimum with a slightly lower energy than the C_{2v} geometry and, each methyl group was rotated so that the closest C–F bond was 20° out of the C–O–C plane. This geometry was supported by gas-phase electron-diffraction experiments by Lowrey et al.,[20] which showed that the C1–F1 and C2–F4 bonds (see Figure 1) were 14° out of the C–O–C plane. Presently, the electron-diffraction data appear to be the best structural data for this system, hence, it is used to compare with the theoretical results. In Table I and II we list the results of a previous calculation[21] using an STO-3G basis set and the present results for the 3-21G, 4-31G, and 6-31G* basis sets; optimized bond lengths are listed in Table I, and the optimized bond angles are listed in Table II; Figure 1 contains computer drawings for different views of the theoretical structure. Figure 1 should also be consulted for the atom labels in order to identify particular bond lengths and angles.

The computed bond lengths and angles obtained by using basis sets larger than the STO-3G are in excellent agreement with experimentally available material. In a previous report[31] optimized geometries for several perfluorinated ethers were computed with use of the STO-3G basis set; due to the size of the systems studied the calculations were constrained to this basis set. As shown by inspection of Tables I and II, the best basis set to use in order to obtain a reliable geometry (at a reasonable cost) is the 3-21G basis; consequently, in this and subsequent reports the structures of perfluoro ethers are investigated at this level.

The most significant result obtained from the theoretical analysis is that the geometry with C_2 symmetry is obtained with

(19) Bürger, H.; Pawelke, G. *Spectrochim. Acta* **1975**, *31A*, 1965.

(20) Lowrey, A. H.; George, C.; D'Antonia, P.; Karle, J. *J. Mol. Struct.* **1980**, *63*, 243.

(21) Pacansky, J.; Liu, B. *J. Phys. Chem.* **1985**, *89*, 1883.

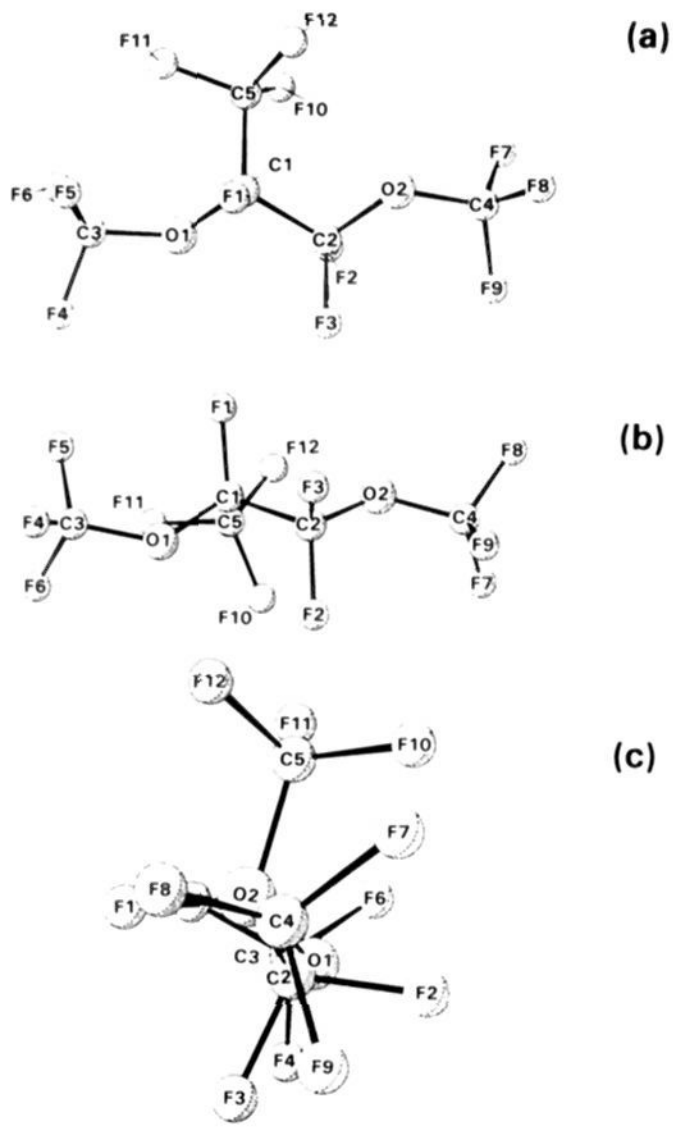

Figure 6. A computer drawing for the optimized geometry of the PPFPO model compound.

Table VII. The Optimized Bond Lengths (Å) for the PPFF Model Compound Obtained with the 3-21G Basis Set

bond	3-21G	bond	3-21G	bond	3-21G
C1–F1	1.336	O1–C2	1.371	C2–F5	1.332
C1–F2	1.336	O2–C3	1.371	C3–F6	1.331
C1–O1	1.374	C2–F3	1.331	C3–F7	1.335
C1–O2	1.374	C2–F4	1.335	C3–F8	1.332

Table VIII. The Optimized Bond Angles (deg) for the PPFF Model Compound Obtained with the 3-21G Basis Set

angle	3-21G	angle	3-21G
O1–C1–O2	111.5	F7–C3–O2	110.7
C2–O1–C1	124.5	F8–C3–O2	111.2
O1–C1–O2	124.5	F1–C1–F2	109.4
C1–O2–C3	109.0	F3–C2–F4	108.5
F1–C1–O1	109.0	F3–C2–F5	109.3
F2–C1–O1	109.0	F4–C2–F5	109.6
F1–C1–O2	109.0	F6–C3–F7	108.5
F2–C1–O2	109.9	F6–C3–F8	109.3
F3–C2–O1	111.2	F7–C3–F8	109.6
F4–C2–O1	110.7	⟨C2–O1–C1⟩ ⟨O1–C1–O2⟩	92.6
F5–C2–O1	107.5	⟨C3–O2–C1⟩ ⟨O2–C1–O2⟩	92.6
F6–C3–O2	111.2		

use of computations ranging from the STO-3G basis to the 6-31G* basis. The angle between the planes formed by the F1–C1–O1 and F4–C2–O1 atoms and the C1–O1–C2 plane is 18°. The perspective shown in Figure 1b shows a view parallel to the C_2 axis while the view in Figure 1c is perpendicular to the C_2 axis clearly revealing the extent of the CF_3 rotation. In addition to the rotation the perfluoromethyl groups are tilted and distorted away from a local C_{3v} symmetry; whereas the F–C–F angles differ slightly, the F–C–O angles differ significantly showing that the tilting is the major distortion away from a local C_{3v} symmetry. The tilt is also encountered in CH_3 groups attached to heteroatoms like nitrogen or oxygen. The rotation, however, is not observed

Table IX. The Optimized Bond Lengths (Å) for the PPFEO Model Compound Obtained with the 3-21G Basis Set

bond	3-21G	bond	3-21G	bond	3-21G
C1–F1	1.347	C2–F4	1.342	C3–F6	1.330
C1–F3	1.342	C2–O2	1.377	C3–F7	1.337
C1–O1	1.377	C3–O1	1.373	C4–F8	1.323
C1–C2	1.506	C4–O2	1.373	C4–F9	1.330
C2–F2	1.347	C3–F5	1.323	C4–F10	1.337

Table X. The Optimized Bond Angles (deg) for the PPFEO Model Compound Obtained with the 3-21G Basis Set

angle	3-21G	angle	3-21G
O1–C1–C2	106.4	F7–C3–O1	110.4
O2–C2–C1	106.4	F8–C4–O2	108.2
C3–O1–C1	124.0	F9–C4–O2	110.7
C4–O2–C2	124.0	F10–C4–O2	110.4
F1–C1–O1	110.6	F1–C1–F3	108.6
F3–C1–O1	111.4	F2–C2–F2	108.6
F2–C2–O2	110.6	F5–C3–F6	109.3
F4–C2–O2	111.4	F5–C3–F7	109.6
F1–C1–C2	109.8	F6–C3–F7	108.6
F3–C1–C2	110.0	F8–C3–F9	109.3
F2–C2–C1	109.8	F8–C3–F10	109.6
F4–C2–C1	110.0	F9–C3–F10	108.6
F5–C3–O1	108.2	⟨C3–O1–C1⟩ ⟨O1–C1–C2⟩	164.5
F6–C3–O1	110.7	⟨C4–O2–C2⟩ ⟨O2–C2–C1⟩	164.5

Table XI. The Optimized Bond Lengths (Å) for the PPFPO Model Compound Obtained with the 3-21G Basis Set

bond	3-21G	bond	3-21G	bond	3-21G
C1–F1	1.359	O2–C4	1.375	C4–F7	1.323
C1–C2	1.515	C2–F2	1.342	C4–F8	1.329
C1–C5	1.518	C2–F3	1.345	C4–F9	1.336
C1–O1	1.392	C3–F4	1.327	C5–F10	1.338
C2–O2	1.379	C3–F5	1.329	C5–F11	1.343
O1–C3	1.371	C3–F6	1.334	C5–F12	1.334

Table XII. The Optimized Bond Angles (deg) for the PPFPO Model Compound Obtained with the 3-21G Basis Set

angle	3-21G	angle	3-21G
O1–C1–C2	106.4	F7–C3–O1	110.4
O2–C2–C1	106.4	F8–C4–O2	108.2
C3–O1–C1	124.0	F9–C4–O2	110.7
C4–O2–C2	124.0	F10–C4–O2	110.4
F1–C1–O1	110.6	F1–C1–F3	108.6
F3–C1–O1	111.4	F2–C2–F2	108.6
F2–C2–O2	110.6	F5–C3–F6	109.3
F4–C2–O2	111.4	F5–C3–F7	109.6
F1–C1–C2	109.8	F6–C3–F7	108.6
F3–C1–C2	110.0	F8–C3–F9	109.3
F2–C2–C1	109.8	F8–C3–F10	109.6
F4–C2–C1	110.0	F9–C3–F10	108.6
F5–C3–O1	108.2	⟨C3–O1–C1⟩ ⟨O1–C1–C2⟩	164.5
F6–C3–O1	110.7	⟨C4–O2–C2⟩ ⟨O2–C2–C1⟩	164.5

for CH_3 groups; plausible causes may be repulsive interactions between lone pairs of electrons on the oxygen and fluorine atoms and/or lone pairs of electrons on the fluorine atoms on each methyl group. The precise origin of this effect is an important topic and will be considered with use of more detailed calculations in another report.

The computed C–F bond lengths also reflect the asymmetry of the CF_3 groups. We note that the C–F bonds closest to the C–O–C plane, C_1–F_2 and C_2–F_4, have the shortest lengths while those twisted farther from the plane have longer but nonequal bond lengths.

As with the perfluorodimethyl ether, perfluorodiethyl ether, $(CF_3CF_2)_2O$, was also found to possess a stable C_2 symmetry. Additional conformations with a planar C–C–O–C–C skeleton were investigated but did not correspond to minima.

Figure 2 contains computer drawings for three different views of the theoretically determined structure, based on the RHF/3-

21G geometry. The atom labeling shown in Figure 2 is that referred to in Tables III and IV. The optimized bond lengths are listed in Table III, and the optimized bond angles are listed in Table IV.

The angle between the planes formed by the C3–C1–O1 and C4–C2–O1 atoms and the C1–O1–C2 plane is about 23°; this compares well with the 18° dihedral angle between the CFO and COC planes in perfluorodimethyl ether. The perspective shown in Figure 2b where the molecule is viewed parallel to the C_2 axis and Figure 1c for a view perpendicular to the C_2 axis clearly reveals the extent of the rotation. On the basis of our studies on perfluorodimethyl ether we expect our computed bond lengths to be within ±0.002 Å for the O–C and C–C bonds and within ±0.01 Å for the CF bonds. The computed C–F bond lengths also reflect the asymmetry of the CF_3CF_2 groups. The C1–F2 and C2–F4 bonds are longer than the C1–F1 and C2–F3 bonds; however, all four CF_2 bond lengths are longer than the CF_3 bond lengths. We should also add that the CF bond lengths in the CF_3 group attached to the oxygen in $(CF_3)_2O$ are slightly shorter than those in the CF_3 group in perfluorodiethyl ether bonded to a carbon. In addition, the CO bond lengths in perfluorodiethyl ether are longer than those in $(CF_3)_2O$.

The optimized geometry for $CF_3OCF_2CF_3$, displayed in Figure 3 and listed in Tables V and VI, is a composite of the $(CF_3)_2O$ and $(CF_3CF_2)_2O$ geometries. Again, the geometry is highlighted by the internal rotation about the C–O bonds imparted by the oxygen–fluorine interactions observed for the two previous systems.

The conformations studied for the poly(perfluoro ether) model compounds were chosen so that they corresponded to the geometry with the lowest energy on the potential energy surface. As shown in Figures 4–6, the presence of the oxygen atom forces the main chain to take on a helical geometry. This is a direct consequence of the C_2 symmetry displayed by the simple ethers above and is very evident for the PPFPO model displayed in Figure 6c. The bond lengths and bond angles for the model compounds contained in Tables VII–XII contain the same structural trends already indicated by the simpler perfluoro ethers. The CF_3 end groups attached to oxygen have about the same bond lengths regardless of the compound. The bond lengths for the CF_2 group attached to two oxygen linkages in PPFF are much shorter than any CF_2 bond lengths encountered; the CF_2 bond lengths in the PPFEO model, however, are about the same length as those in the PPFPO model and $(CF_3CF_2)_2O$. The C–F bond lengths in the CF_3 group in the PPFPO model have lengths about that computed for perfluorodiethyl ether. The tertiary CF bond and the C–C and C–O bond lengths in the PPFPO model are quite interesting; the tertiary CF bond length of 1.359 Å is the longest CF bond encountered in the present studies. The bond lengths for C–O bonds connecting terminal CF_3 groups and those in $(CF_3)_2O$, $(CF_3CF_2)_2O$, and $CF_3OCF_2CF_3$ have about the same length, 1.370–1.378 Å. The bond length for the C–O bond attaching the tertiary carbon, C1, in PPFPO, to O1 is 1.392 Å, which is a direct reflection of the relatively weaker bonds around this carbon atom; both of the C–C bonds attached to the tertiary carbon also reflect this because their computed bond lengths are calculated at C1–C2 = 1.515 Å and C1–C5 = 1.518 Å, which is about 0.01 Å longer than those C–C bond lengths in the other compounds studied herein.

Other important results of the theoretical study are the molecular orbital energies, the molecular orbital plots, and the net charge on each of the atoms in the molecule. Due to the number of electrons in the $(CF_3)_2O$ system, only the HOMO (highest occupied molecular orbital) and LUMO (lowest unoccupied molecular orbital) will be discussed. These are the most important because of their chemical and spectroscopic relevance. In Figure 7, pertinent molecular orbital energy levels are plotted while Figure 8a–f contains orbital plots for the HOMO and LUMO of each system. The HOMO for $(CF_3)_2O$ for the most part consists of a nonbonding pair of electrons that reside in a p-orbital on the oxygen atom with lobes antisymmetric to the C–O–C plane; the HOMO also contains a modest but much smaller contribution from lone pairs on the fluorine atoms. The LUMO (Figure 8a)

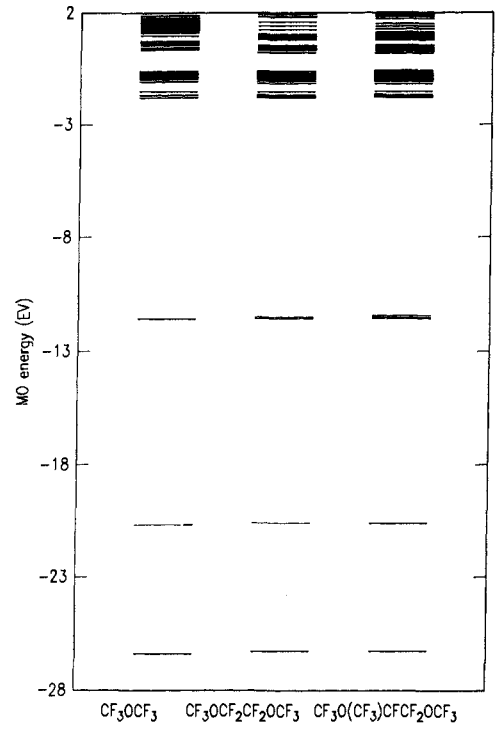

Figure 7. Molecular energy levels for (a) perfluorodimethyl ether, (b) perfluorodiethyl ether, and (c) the PPFPO model compound.

is an antibonding molecular orbital with respect to the C–O bonds. An electronic excitation from the HOMO to the LUMO may thus be viewed as an excitation where charge is moved from a nonbonding lone pair on oxygen to regions between the C–O bonds which in effect leads to weakening of the C–O and C–F bonds.

Figure 8b contains the orbital plots for the HOMO and LUMO of the $(CF_3CF_2)_2O$ system. The HOMO consists of an equal admixture of the nonbonding pair of electrons which reside in a p-orbital on the oxygen atom, with lobes antisymmetric to the C–O–C plane, and a C–C σ bond in the perfluorodiethyl groups; the HOMO also contains a modest but much smaller contribution from lone pairs on the fluorine atoms. The LUMO is an antibonding molecular orbital with respect to the C–O bonds. In this case, an electronic excitation from the HOMO to the LUMO may thus be viewed as an excitation where charge is moved from the nonbonding lone pair on oxygen to regions between the C–O bonds which in effect leads to weakening of the C–O and C–F bonds.

The orbital plots for the HOMO and LUMO of $CF_3OCF_2CF_3$, shown in Figure 8c, are composites of the orbital plots of the perfluorodimethyl and perfluorodiethyl ether systems.

The orbital plot for the HOMO and LUMO of the PPFF model compound are shown in Figure 8d. The HOMO consists of a small contribution from nonbonding electrons in fluorine p-orbitals; however, the major contribution is again from lone pairs of electrons residing in oxygen p-orbitals, and hence may be viewed as a nonbonding orbital. The LUMO shows that every C–O bond in the system is antibonding as indicated by the p-orbitals directed toward each other with opposite phases.

The HOMO for the PPFEO model compound (Figure 8e) again consists of a small contribution from lone pairs of electrons in fluorine p-orbitals; the primary contribution, however, is due to the lone pairs of electrons in oxygen p-orbitals and the C–C bond. The LUMO has a very different character from all of the other systems studied in this report; it is best described as an antibonding C–C orbital. Thus, in this case, excitation of an electron from the HOMO to the LUMO also leads to a weakening of the C–C bonds.

The orbital plots for the PPFPO system drawn in Figure 8f track along the same lines as the previous systems. For example, the HOMO is a mixture of a lone pair of nonbonding electrons in p-orbitals on the oxygen attached to the tertiary carbon and

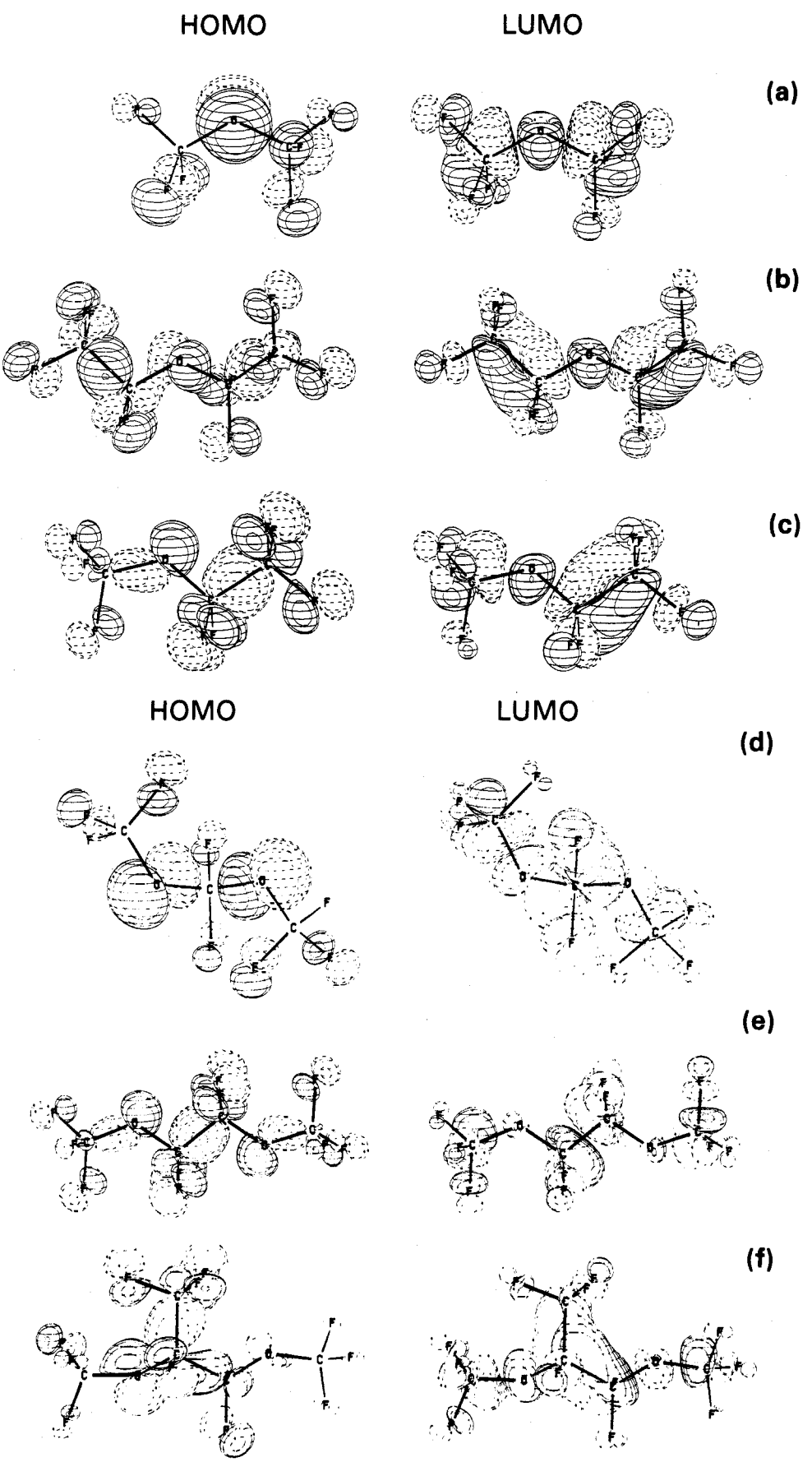

Figure 8. Orbital plots for the HOMO and LUMO of (a) perfluorodimethyl ether, (b) perfluorodiethyl ether, (c) perfluoromethyl perfluoroethyl ether, (d) the PPFF model compound, (e) the PPFEO model compound, and (f) the PPFPO model compound.

the lone pair of electrons on the second oxygen atom which contributes negligibly; in addition, the HOMO also consists of the C–C bond connecting the CF_3 group, the C–C in the main chain, and a smaller amount of contribution from nonbonding

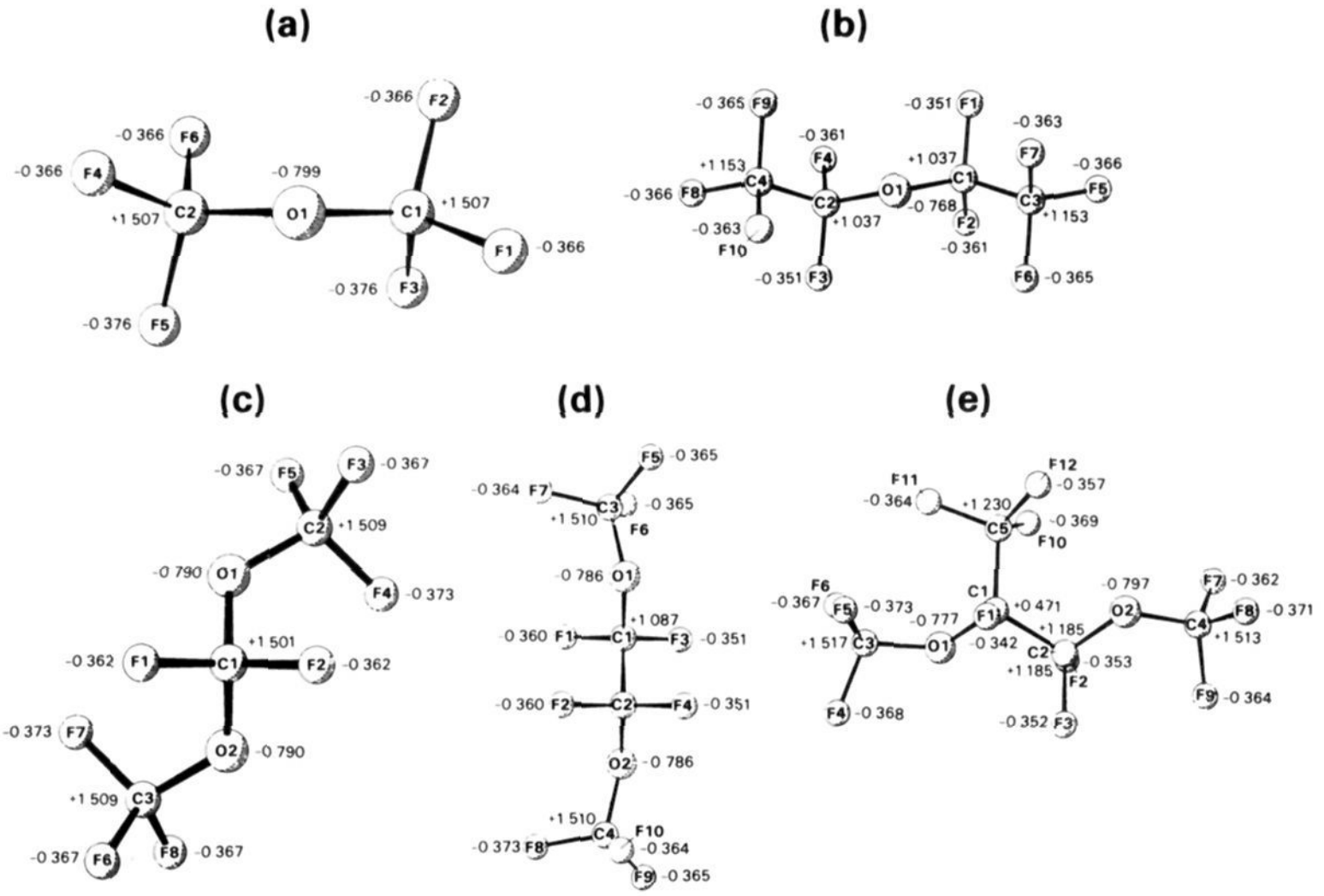

Figure 9. The net charge distributions for (a) perfluorodimethyl ether, (b) perfluorodiethyl ether, (c) the PPFF model compound, (d) the PPFEO model compound, and (e) the PPFPO model compound.

Figure 10. The conformation obtained for poly(perfluoroformaldehyde), $CF_3CF_2O-(CF_2O-)_{20}CF_2CF_3$, with molecular mechanics.

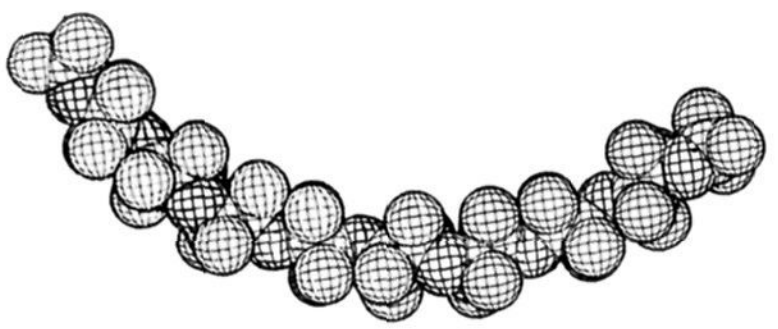

Figure 11. The conformation obtained for poly(perfluoroethylene oxide), $CF_3CF_2O-(CF_2CF_2O-)_{20}CF_2CF_3$, with molecular mechanics.

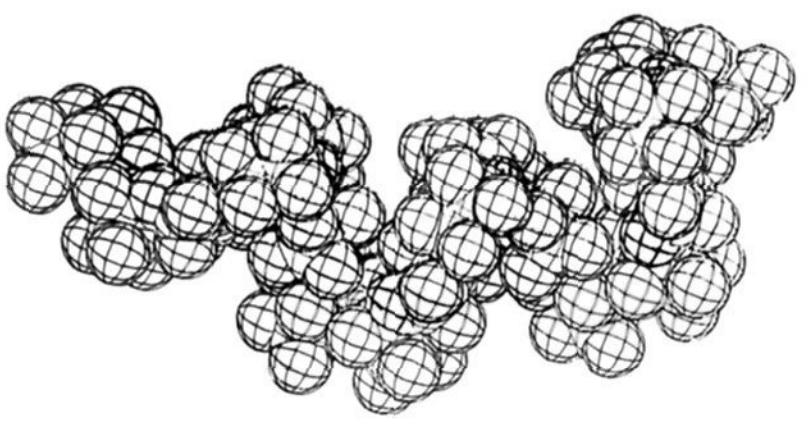

Figure 12. The conformation obtained for poly(perfluoropropylene oxide), $F-(CF_3CFCF_2O-)_{20}CF_2CF_3$, with molecular mechanics.

electrons on the fluorine atoms on the CF_3, CF_2 groups and the fluorine attached to the tertiary carbon. The orbital plots for the LUMO in PPFPO indicate extensive antibonding in all of the CO bonds.

The Mulliken net charge on each atom is one of the most revealing results of the theoretical analysis for perfluoro ethers. As shown in Figure 9, due to the extreme electron-withdrawing power of fluorine and oxygen, each fluorine atom has an excess negative charge of $\simeq$0.37 e while the oxygen is negatively charged by $\simeq$0.79 e. The net gain in charge by the oxygen and fluorine atoms is matched by a severe loss of charge by the carbon atoms; most carbon atoms are positive by $\simeq$1 to 1.5 e. The only exception here is the tertiary carbon in the PPFPO model which has lost about 0.47 e. As a result the C–O bonds are very polar and susceptible to attack by Lewis acids and bases; consequently, perfluoro ethers exhibit, for example, catalysis when in contact with metal oxides. It has been reported[22] that the PPFEO, PPFF type polymers have lower thermal-oxidative stability compared to PPFPO-type materials. This is surprising since the tertiary CF bonds in PPFPO are weaker than the secondary or primary CF bonds in PPFF and PPFEO. (The theoretical analysis also predicts that the branched materials have less thermal stability by the long tertiary CF bond length in PPFPO and, as shown below, the weaker tertiary CF bond stretching force constant.) Jones[23] has shown that the linear polymers are inherently unstable at 316° in an oxidizing atmosphere which cannot be attributed to hydrogen chain termination or residual peroxide linkages. In the presence of a metal catalyst in oxidizing atmospheres the unbranched polymers exhibit much greater degradation than in uncatalyzed tests; however, these catalysts do not promote degradation at 316 °C in an inert nitrogen atmosphere. In addition, catalyzed tests indicated that pure metals did not promote as much degradation as alloys. Again, as with the PPFPO materials, the metals and alloys promoted degradation by a chain scission process.

A reasonable explanation for the increased catalytic activity of the unbranched systems, which also tends to explain the large

(22) For an account on thermal stability of perfluorinated ethers see: Jones, W. R., Jr. In *New Directions in Lubrication, Materials, Wear, and Surface Interactions*; Loomis, W. R., Ed.; Noyes Publication: Park Ridge, New Jersey, 1985; pp 402–437.

(23) Jones, W. R., Jr. NASA TM-82834, Apr 1982.

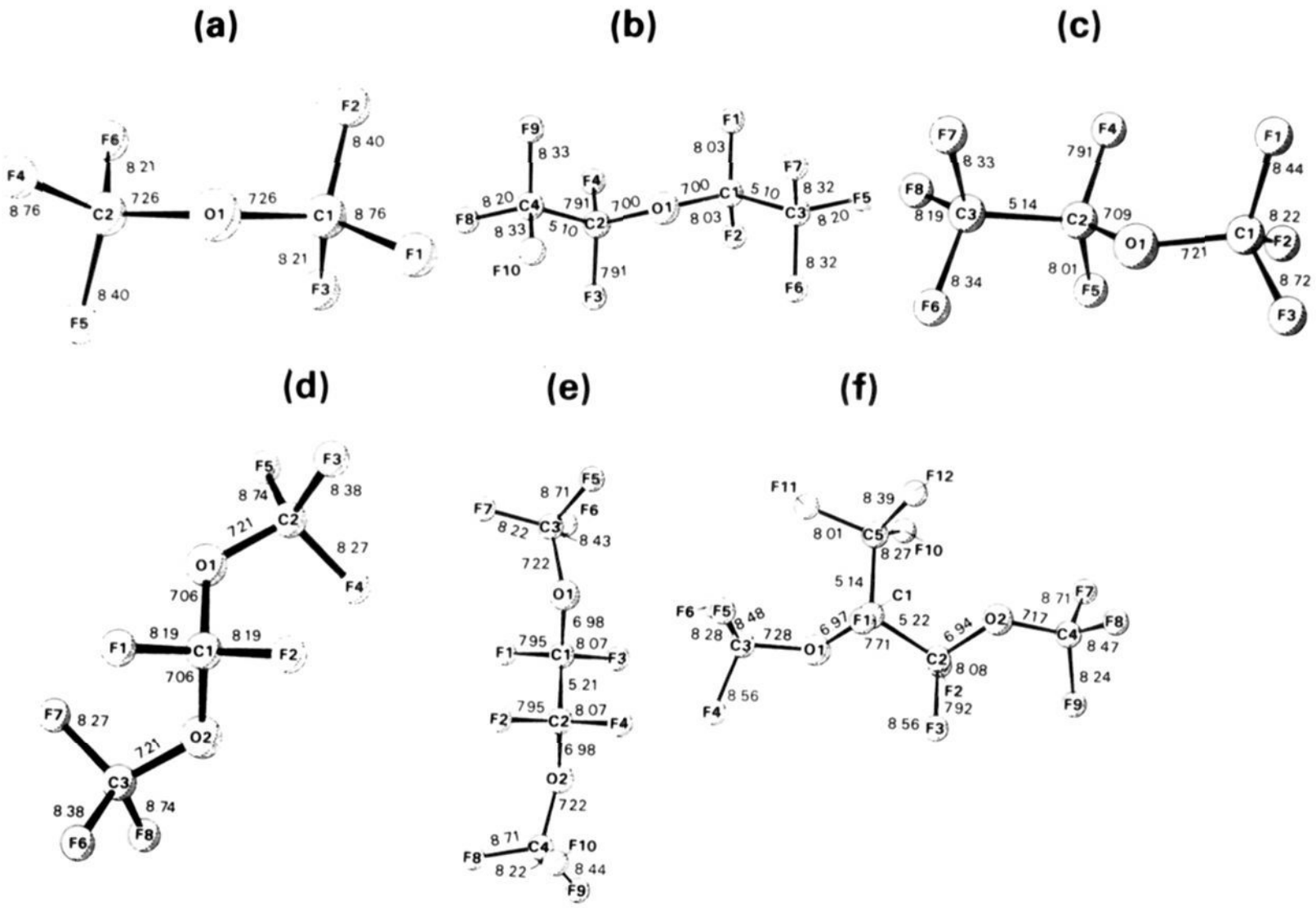

Figure 13. The bond stretching force constants (mdyn/Å) for $(CF_3)_2O$, $(CF_3CF_2)_2O$ and the PPFF, PPFEO, PPFPO model compounds.

differences in viscosities of PPFPO and PPFEO-PPFMO copolymers, begins with the structures contained in Figures 10–12, net charges, and the fact that the electronic distribution in the ground states is dominated by lone pairs of electrons on oxygen. (Lone electron pairs on fluorine residue in orbitals with much lower energies and hence are not as important chemically.) The structures shown in Figures 10–13 were obtained with use of optimized geometries given herein and molecular mechanics techniques (Allinger's MM2 code with supplemental parameters); the structures shown with the particular number of monomeric structures is merely a reflection of what can be represented with decent clarity in a figure. We first note that the helical nature of the geometry is a direct consequence of the rotation about the C–O bonds imparted by the interaction between lone pairs of electrons on fluorine and oxygen. The PPFF polymer chain may be viewed as a helical chain of oxygen lone electron pairs; furthermore, the net charge on each oxygen is excessively negative. This trend continues for PPFEO, but it abruptly changes for PPFPO where now, as shown in Figure 12, although the oxygen atoms still have a rather large negative net charge, the CF_3 side chains tend to shield the oxygen lone electron pairs, and hence the polar C–O bond. (Recall that the fluorine lone electron pairs reside in much lower energy levels and thus shield the oxygen lone pairs.) We tend to accept this as an explanation for why the unbranched polymers are more susceptible to catalyst and hence exhibit less thermal stability on metal and metal oxide surfaces.

A first indication of the thermal stability of perfluoro ethers and hence bond strengths is bond stretching force constants. These are collected in Figure 13 alongside of the respective bond in each molecular system. A number of generalizations are apparent. The stretching force constants range from $\simeq$8 for CF bonds, to $\simeq$7.3 for CO bonds, and to $\simeq$5.2 for CC bonds; it is reasonable to expect the bond energies to follow the same trend.

The range of values for the CF bond stretches is the most interesting. They are the highest for CF bonds in CF_3O ($\simeq$8.8), about 8.2 for CF bonds in CF_3C, and about 8.0 for CF bonds in CF_2 groups; the lowest value is for the tertiary CF bond in the PPFPO model compound, $\simeq$7.7. Hence, in one perfluorinated ether, PPFPO, as indicated by the calculated force constants for the PPFPO model, we find a very large range in CF bond stretching force constants and a relatively weak CF bond.

Another important feature is the wide range for the CF force constants for CF_3 when attached to an oxygen atom relative to the CF_3 attached to a carbon. For example, examine the force constants for perfluoromethyl perfluoroethyl ether which contains CF_3 groups in both types of environments. The CF force constant for the C1–F3 bond, which is closest to the C1O1C2 plane, has the highest value, 8.72; the bond trans to the lone pair of electrons on the oxygen has the lowest value 8.22. The CF bond force constants, although not identical, have a smaller range for the CF_3 group attached to the carbon. In essence, this is a valuable

Table XIII. The Calculated Vibrational Frequencies (cm^{-1}) for Perfluorodimethyl Ether Obtained with the 3-21G, 4-31G, and 6-31G* Basis Sets

vib	symm	3-21G	4-31G	6-31G*
21	A	1568.35 a	1496.09	1529.46
20	B	1510.99 b	1436.05	1461.47
19	B	1469.64 b	1410.14	1457.28
18	A	1451.30 b	1376.66	1443.92
17	A	1423.47 b	1369.11	1411.15
16	B	1378.27 b	1346.61	1374.22
15	B	1054.59 c	1030.21	1083.23
14	A	901.77 d	881.14	951.58
13	A	786.81	770.52	818.60
12	B	714.93 e	703.13	755.04
11	B	702.62 f	689.67	724.27
10	A	610.18	599.40	638.15
9	B	593.43	582.40	621.97
8	A	548.28	535.56	576.51
7	B	488.01	479.89	514.55
6	A	380.20	373.72	398.69
5	B	371.42	367.26	391.13
4	A	366.85	355.24	379.34
3	A	161.14	157.30	184.84
2	A	55.51	75.11	101.57
1	B	51.88	35.67	43.45

Table XIV. The Calculated Infrared Vibrational Intensities (km/mol) for Perfluorodimethyl Ether Obtained with the 3-21G, 4-31G, and 6-31G* Basis Sets

vib	symm	3-21G	4-31G	6-31G*
21	A	426.11	421.20	632.11
20	B	710.83	709.28	746.04
19	B	718.43	934.89	115.79
18	A	0.17	171.26	817.12
17	A	270.91	102.83	2.36
16	B	673.42	418.98	440.65
15	B	39.97	61.47	69.17
14	A	6.49	2.98	0.00
13	A	0.36	0.07	1.58
12	B	71.76	68.92	41.26
11	B	47.79	43.04	16.70
10	A	0.00	0.00	0.00
9	B	14.87	12.52	6.36
8	A	13.51	13.53	6.24
7	B	0.93	0.99	0.60
6	A	0.32	0.22	0.00
5	B	0.94	0.61	0.41
4	A	0.00	0.00	0.00
3	A	0.75	1.09	0.59
2	A	0.01	0.01	0.02
1	B	0.01	0.00	0.00

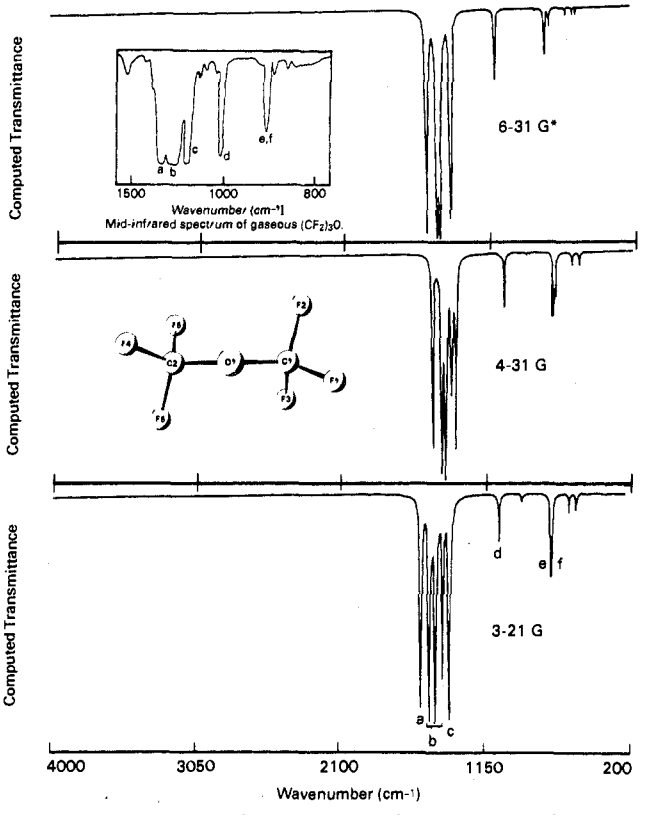

Figure 14. A comparison of the computed infrared spectrum of $(CF_3)_2O$ with the observed gas-phase spectrum.[24] An assignment is given for a number of important spectral features in the theoretical spectrum: a. ν(C1F1) + ν(C2F4); b, $\nu(CF_3)$; c, ν_a(CO); d, $\nu(CF_3)$; e, $\alpha(CF_3)$; f. α-(CF_3) + β(FCO). ν is defined as a bond stretch. and α and β are valence angle bends.

analytical and structural aid because the vibrational frequencies associated with a CF_3O will be different from those associated with a CF_3C group, and as a result they may be used to identify the presence of such groups in a molecule.

The force constants for the C–O bonds are the largest for CF_3O bonds, $\simeq$7.26, and the lowest for the C–O bond to the tertiary carbon atom in the PPFPO compound, C1O1. The C–C bond force constants have the smallest range from $\simeq$5.22 for the CF_3C group in the PPFPO model to 5.10 in diethyl ether.

Vibrational spectroscopy is frequently used to investigate structure and interactions of perfluorinated ethers in contact with surfaces. Pertinent examples are the use of perfluorinated lubricants in the magnetic media industry and their use in vacuum systems as both lubricants and pump oils. While vibrational spectroscopy is convenient, vibrational spectra of perfluorinated ethers are difficult to interpret; natural band widths are very large, making it difficult to resolve spectral features, and since fluorine does not have isotopes a normal mode analysis is almost impossible. In this case theory is able to provide detail not available via experiment; hence we present calculated and experimental infrared spectra for the purposes of assigning salient infrared bands. In subsequent reports, we will detail the vibrational analysis; here, we intend to present detail sufficient to obtain an overview for a wide number of systems.

Table XV. The Vibrational Frequencies and Intensities for Perfluorodiethyl Ether

vib no.	vib symm	vib freq, cm^{-1}	vib freq scaled (0.89)	computed IR inten, km/mol
39	A	1561.13	1389.41 a	2.44
38	B	1532.88	1364.26 b	35.09
37	B	1469.34	1307.71 c	903.87
36	A	1454.69	1294.68 c	181.94
35	B	1448.74	1289.38 c	373.69
34	A	1448.23	1288.92 c	151.86
33	B	1410.66	1255.48 d	66.41
32	A	1395.77	1242.24 d	28.97
31	A	1363.09	1213.15 e	267.86
30	B	1339.99	1192.59 f	430.15
29	B	1233.76	1098.04 g	346.91
28	A	1219.66	1085.50 h	113.42
27	B	874.71	778.49 i	14.68
26	A	869.95	774.26	3.14
25	A	785.40	699.00 j	27.87
24	B	726.07	646.20 k	129.6
23	B	686.20	610.72	8.80
22	B	657.88	585.51	14.81
21	A	638.77	568.50	4.24
20	A	604.58	538.08	0.46
19	B	577.93	514.361	23.53
18	A	562.04	500.22 m	20.93
17	B	541.34	481.80 n	33.46
16	A	480.16	427.34	2.50
15	B	420.91	374.61	1.04
14	B	386.93	344.36	1.06
13	A	383.21	341.05	0.11
12	A	332.70	296.10	0.10
11	B	322.58	287.10	6.49
10	A	315.76	281.02	2.04
9	A	228.91	203.73	1.17
8	B	224.93	200.19	9.40
7	A	198.96	177.08	0.02
6	B	191.38	170.33	2.42
5	A	90.74	80.76	0.73
4	B	78.54	69.90	0.22
3	A	61.09	54.37	0.05
2	A	37.62	33.48	0.00
1	B	37.50	33.38	0.05

First here are some general comments: the IR absorptions of poly(perfluorinated ethers) are very broad, all have bands in the 1400–1000-cm^{-1} region with several much weaker features at $\simeq$800 to 500 cm^{-1}. In some cases bands can be partially resolved but in most cases the natural band widths are too large to permit a separation.

The calculated vibrational frequencies and infrared intensities for $(CF_3)_2O$ are listed in Tables XIII and XIV according to the basis set used to judge the effect of using a 3-21G basis set. The largest basis set, the 6-31G*, gives the best results but could not be used for the larger model compounds. We note that the 3-21G basis does give reasonable results and its use is thus justified. In order to present this further the calculated infrared spectrum is compared to the gas-phase infrared spectrum reported by Durig and coworkers.[24] The computed spectrum was simulated with use of a Lorentzian function for each band and the band widths

(24) Witt, J. D.; Durig, J. R.; DesMarteau, D.; Hammaker, R. M. *Inorg. Chem.* **1973**, *12*, 807.

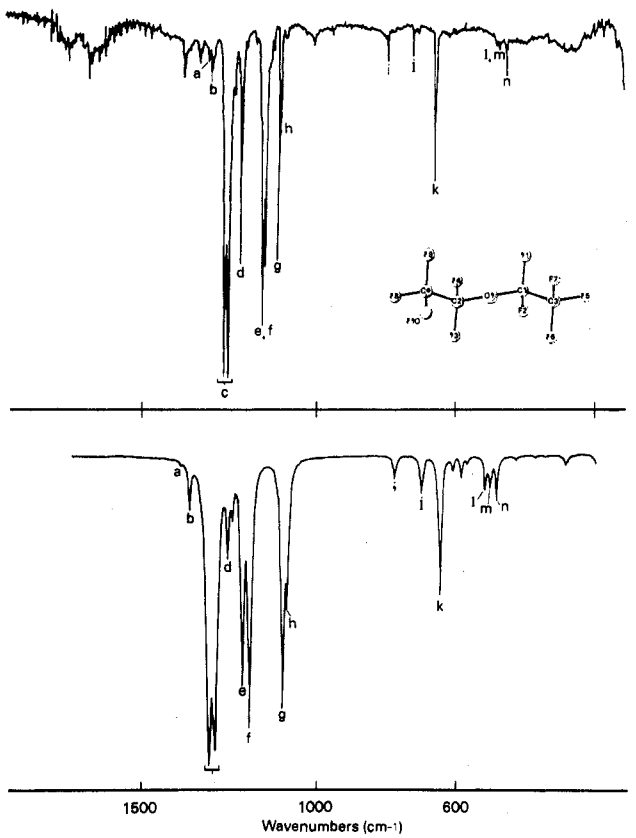

Figure 15. A comparison of the computed infrared spectrum of $(CF_3CF_2)_2O$, with the infrared spectrum obtained in solid argon (concentration: 1/10000) at $T = 10$ K. Band assignments are made on the basis of the theoretical spectrum: a, ν_s(CC); b, ν_a(CC); c, $\nu(CF_3)$; d, $\nu(CF_2)$; e, ν_s(CO); f, ν_a(CO); g, $\nu(CF_3) + \nu(CF_2)$; h, ν_s(CO) + $\nu(CF_3)$; i, ν_a(CC) + $\nu(CF_3) + \nu(CF_2)$; j, ν_s(CC) + $\nu(CF_2)$; k, ν_a(CC) + $\alpha(CF_3) + \alpha(CF_2)$; l, α(C2O1C1) + $\alpha(CF_2) + \alpha(CF_3)$; m, $\alpha(CF_2) + \alpha(CF_3)$; n, $\alpha(CF_2) + \alpha(CF_3)$. ν is defined as a bond stretch, and α is a valence angle bend.

were all set equal; this procedure is only intended for qualitative arguments, and to match the computed with the observed spectrum as closely as possible.

As shown in Figure 14, all basis sets reproduce the experimental spectrum; the 6-31G* provides the best fit as indicated by the band intensities in the lower frequency region. The labels on the 3-21G spectrum refer to band assignments based on normal mode displacement vectors and potential energy distributions, PED;[25] the latter furnishes information on the contribution of each force constant to the normal frequencies of vibration. In general, the spectra consists of bands for stretching frequencies, referred to as ν(CF) for example, and bending modes referred to as either $\alpha(CF_2)$ or $\beta(CF_2)$, i.e., valence angle bends and or rocking and wagging motions. For $(CF_3)_2O$ the order from high to lower frequency is ν(CF) > ν(CO) > $\alpha(CF_3)$. As far as the intensities are concerned, the order from strong to weaker absorption is ν(CO) > ν(CF) >>> valence angle bends, rocks, and wags. This pattern holds for all of the perfluorinated materials considered in this report.

The band labeled a in Figure 14 is a ν(CF) mode for the stronger CF bonds C1F1 and C2F4. CF_3 groups bonded to carbon do not display this, at least to the magnitude shown here. The next three intense bands are stretching frequencies for all of the CF bonds in the methyl group. The intense feature c is ν_a(CO), the asymmetric stretching of the C–O bonds which in hydrocarbon spectra are also observed as very intense absorptions. The band labeled d involves a strongly coupled stretching motion of all of the CF bonds and may in fact be a fingerprint for this molecule; as shown below other systems have similar types of motions involving a complicated stretching of a large part of the molecule. The bands labeled e and f are coupled vibrational modes involving valence angle bends coupled with rocking and twisting motions; this band appears to be characteristic for CF_3 groups attached to oxygen.

(25) Califano, S. *Vibrational States*; John Wiley and Sons: New York, 1976.

XVI. The Computed Vibrational Frequencies and Intensities for the PPFPO Model Compound

vib no.	vib symm	vib freq, cm^{-1}	vib freq scaled (0.89)	computed IR inten, km/mol
51	A	1542.36	1372.70 a	284.25
50	A	1511.39	1345.14 b	618.29
49	A	1505.44	1339.84 b	285.63
48	A	1493.79	1329.48 c	335.76
47	A	1492.45	1328.28 c	569.59
46	A	1463.87	1302.85 d	323.20
45	A	1455.19	1295.12 d	109.80
44	A	1449.49	1290.05 d	284.23
43	A	1397.16	1243.47 e	41.21
42	A	1371.81	1220.91 f	504.83
41	A	1368.75	1218.19 f	1039.16
40	A	1363.79	1213.77 f	75.40
39	A	1333.81	1187.09 g	132.55
38	A	1271.36	1131.51 h	71.20
37	A	1102.10	980.86 i	162.46
36	A	1005.84	895.20 j	13.05
35	A	921.20	819.86 k	14.79
34	A	872.73	776.73 l	31.02
33	A	821.12	730.80 m	20.41
32	A	754.51	671.51 n	37.98
31	A	733.52	652.83	0.45
30	A	690.59	614.62 o	45.57
29	A	664.84	591.71 p	66.37
28	A	656.02	583.86 g	68.45
27	A	643.24	572.48	3.78
26	A	634.26	564.49	7.82
25	A	579.73	515.96	16.90
24	A	561.85	500.05	29.96
23	A	553.67	492.76	2.80
22	A	548.37	488.05	14.84
21	A	490.19	436.27	5.70
20	A	468.29	416.78	0.71
19	A	412.01	366.69	1.57
18	A	376.69	335.26	0.32
17	A	358.69	319.23	0.64
16	A	351.57	312.89	4.28
15	A	334.85	298.01	1.26
14	A	327.80	291.74	1.39
13	A	277.61	247.07	5.62
12	A	244.77	217.85	0.34
11	A	224.23	199.56	1.33
10	A	215.99	192.23	3.56
9	A	190.18	169.26	1.31
8	A	159.94	142.35	0.22
7	A	98.90	88.02	0.15
6	A	81.40	72.45	0.01
5	A	74.18	66.02	0.12
4	A	68.65	61.10	0.20
3	A	45.61	40.59	0.00
2	A	34.23	30.46	0.02
1	A	20.44	18.19	0.02

The calculated vibrational frequencies and infrared intensities for $(CF_3CF_2)_2O$ are contained in Table XV; these and subsequent band centers and intensities are all computed with use of the 3-21G basis. The experimental and theoretical spectra are shown in Figure 15; the labels are the best possible assignments again based on the normal mode displacement vectors and PED obtained theoretically. The reader should be aware that vibrational modes for perfluorinated ethers are highly coupled and it is very difficult to uniquely define the motion as a "pure" CF or C–O stretch, especially as the number of vibrational modes increases. All of the analysis that follows is subject to this, but nevertheless, the "best" possible assignment and description is given.

The infrared spectrum for $(CF_3CF_2)_2O$ in solid argon is characterized by intense absorptions due to ν(CF) and ν(C–O) modes and the weaker absorptions due to the valence angle bending

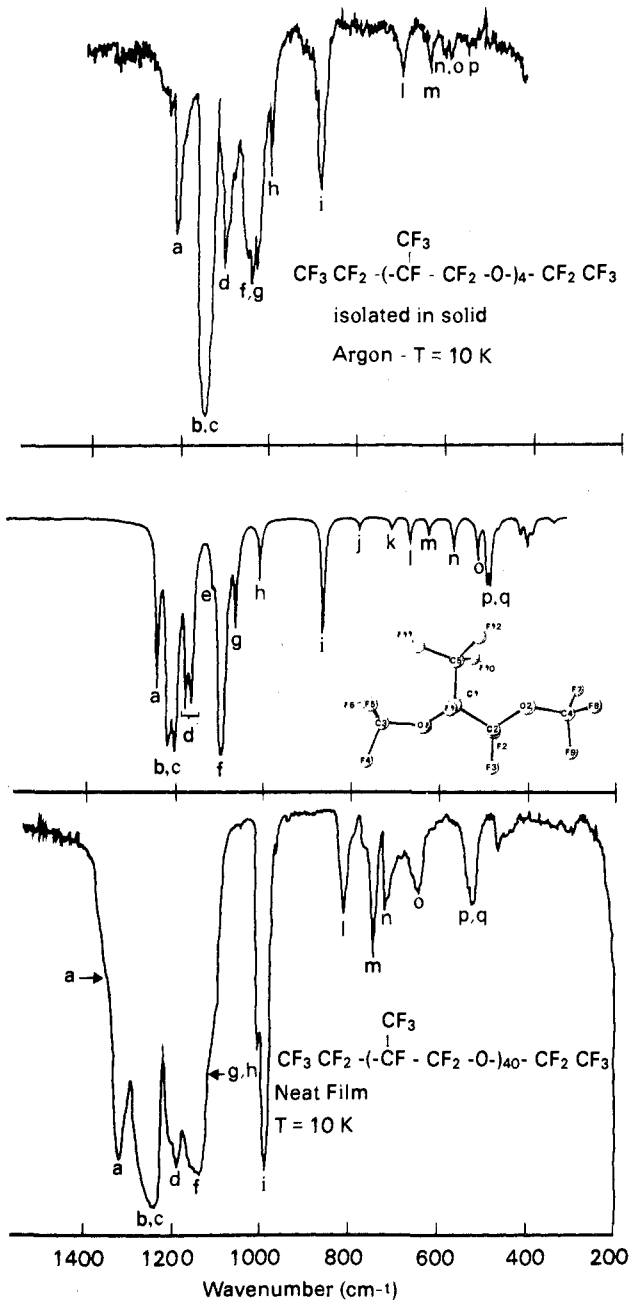

Figure 16. The infrared spectrum of a thin film of CF_3CF_2O–$(CF_3CF$-CF_2O–$)_4CF_2CF_3$, and PPFPO [CF_3CF_2O–$(CF_3CFCF_2O$–$)_{40}CF_2CF_3$]. The spectra were recorded with the sample temperature at T = 10 K. The computed infrared spectrum for the PPFPO model compound is also shown along with an assignment for the salient bands. The oligomer and polymer absorptions labeled by a letter have been assigned to particular vibrational motions on the basis of the model compound: a, ν(C1C2) + $\nu(CF_2)$ + $\nu(CF_3)$; b, $\nu(CF_2)$ + $\nu^e(CF_3)$; c, ν(C1C5) + $\nu^e(CF_3)$; d, $\nu^s(CF_3)$ + ν(C1C5) + ν(C1C2); e, $\nu(CF_2)$; f, ν(C3O1) + ν(C4O2); g, ν(C1F1) + ν(C1O1) + ν(C2O2); h, ν(C1O1) + ν(C1F1); i, ν(C1C5) + ν(C1C2) + $\nu(CF_2)$ + $\nu^s(CF_3)$; j, sym (ν(C3Oi) + ν(C4O2)) + $\nu^e(CF_3)$; k, asym (ν(C3O1) + ν(C4O2)) + $\nu^e(CF_3)$; l. ν(C2O2) + ν(C4O2) + $\nu(CF_2)$ + $\nu^e(CF_3)$; m, ν(C1O1) + ν(C3O1) + ν(C5C1) + ν(C1F1) + $\nu^s(CF_3)$; n. $\nu^s(CF_3)$ + α(C2C1C5) + β(F1C1O1) + $\alpha^s(CF_3)$; o. $\nu^s(CF_3)$ + $\alpha(CF_2)$; p, ν(C4O2) + α(C2C1C5) + β(C2C1O1) + β(F1C1O1); q, $\nu^e(CF_3)$ + $\alpha^e(CF_3)$; ν is defined as a bond stretch, α and β are valence angle bends.

motions in the lower frequency part of the IR. As shown by the theory–experiment comparison in the figure, the agreement is excellent even at the 3-21G level. Hence, we are able to assign the important bands; these are labeled on both spectra, and are also listed in Table XV. Note that more than one mode may be assigned to a band labeled by a letter; the intent here is to simulate the experimental spectrum; consult Table XV for further documentation. The modes with the highest frequencies are marked a and b and are due to symmetric and asymmetric stretching motions of the C–C bonds, ν_s(CC), and ν_a(CC). As shown in Table XV the ν(CC) motions inherently have weak intensities but the highest frequencies. Those bands labeled c are due to $\nu(CF_3)$ in the methyl groups and characteristically absorb strongly in the IR. Slightly lower in frequency are bands labeled d, which are attributed to $\nu(CF_2)$, i.e., CF stretches involving the methylene groups. The relatively intense features marked e and f are due to symmetric and antisymmetric motions of the C–O bonds, ν_s-(CO) and ν_a(CO). Those bands labeled g, h, i, and j are due to coupled stretching motions of the C–O, C–C, and C–F bonds; a band for a similar type of motion was found in $(CF_3)_2O$. In particular the intense band g, which consists of a coupled $\nu(CF_3)$, $\nu(CF_2)$ mode, may also serve as a useful fingerprint, along with h, a coupled stretching of the ν(CO) and $\nu(CF_3)$ bonds. The bands i and j are stretches involving the ν_a(CC), $\nu(CF_3)$, $\nu(CF_2)$, and ν_s(CC), $\nu(CF_2)$ motions, respectively. The valence angle bending motion involving the methyl and methylene groups is assigned to the spectral feature labeled k; l, m, n are strongly coupled motions involving CF_3, CF_2, and C–O–C valence angle bends.

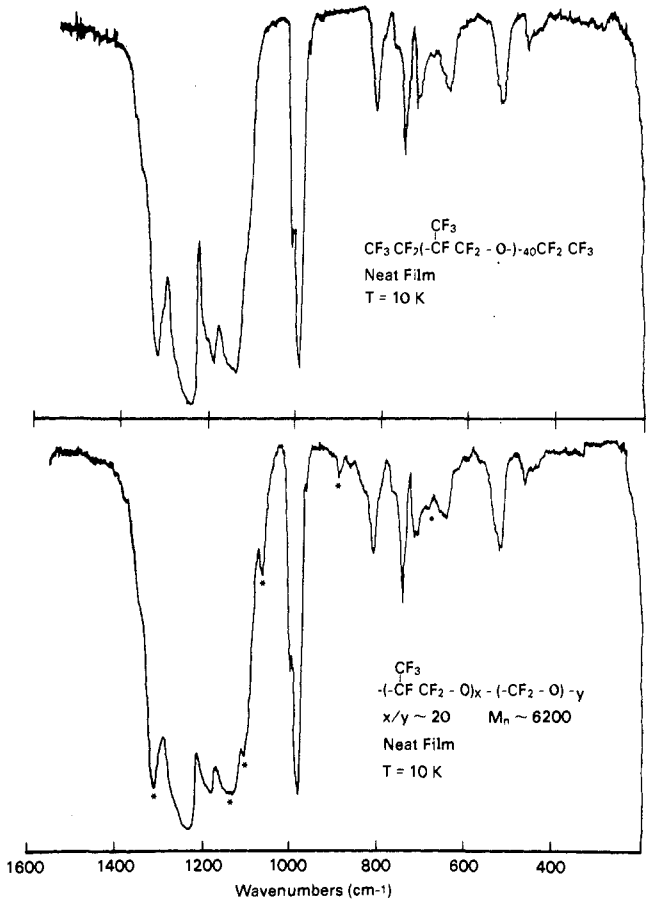

Figure 17. The transmission infrared spectrum of a thin film of PPFPO [CF_3CF_2O–$(CF_3CFCF_2O$–$)_{40}CF_2CF_3$] compared with the thin film spectrum of the PPFFPFPO copolymer [CF_3CF_2O–$(CF_3CFCF_2O$–$)_y$–$(CF_2O)_x$–CF_2CF_3]. The spectra were recorded with the sample temperature at T = 10 K. The additional features exhibited by the copolymer spectrum are marked by an asterisk and are due to the –(CF_2O) units.

The assignment of the vibrational spectrum for PPFPO was studied by recording infrared spectra of a PPFPO tetramer in an argon matrix and of a thin film of PPFPO at T = 10 K and then comparing this to the calculated IR spectrum. Table XVI contains the calculated vibrational frequencies and intensities while Figure 16 shows a comparison of all three spectra. Refer to Table XVI for a clearer picture of the bands labeled in Figure 16. As shown in Figure 16 the theoretical spectrum is in excellent agreement with the PPFPO oligomer IR spectrum, and as a result it may

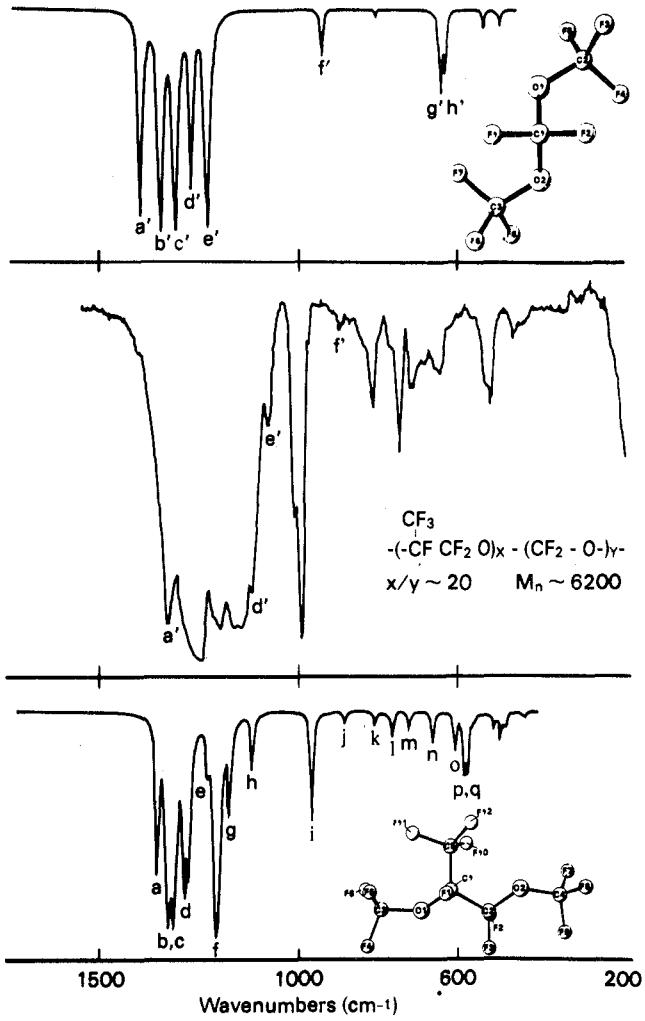

Figure 18. The infrared spectrum of PPFFPFPO copolymer compared to the calculated infrared spectra of the PPFPO and PPFEO model compounds. The copolymer absorptions labeled by a letter have been assigned to particular vibrational motions on the basis of the two model compounds: a', $\nu(CF_2) + \nu(CF_3)$; b', $\nu(CF_3)$; c', $\nu(CF_3)$; d', $\nu(CF_2) + \nu(C1O1) + \nu(C1O2)$; e', $\nu(C1O1) + \nu(C1O2) + \nu(C2O1) + \nu(C3O2)$; f', $\nu(C2O1) + \nu(C2O2) + \nu(CF_3)$; g', $\beta(F1C1O2) + \alpha(CF_3)$; h', $\alpha(CF_2) + \beta(O1C1O2)$. ν is defined as a bond stretch, and α and β are valence angle bends.

be used to make credible assignments for the polymeric PPFPO spectrum. Although the IR spectrum of the latter was taken with the sample at $T = 10$ K, the bands are still not entirely resolvable; this is a direct consequence of the large number of coupled oscillators per PPFPO molecule, somewhat characteristic of polymeric materials.

The bands labeled a in Figure 16 are due to ν(C1C2) modes with some $\nu(CF_2)$ and $\nu^e(CF_3)$ contributing; here, we distinguish between methyl groups on the ends of the molecule attached to O1 and O2 with a superscript e and the methyl forming the side chain with a superscript s. The intense bands b and c are $\nu(CF_2)$ and ν(C1C5) motions, respectively, each with some CF stretching from the CF_3 end groups, $\nu^e(CF_3)$. The absorption, d, is primarily a CF stretching mode involving the side chain $\nu^s(CF_3)$ coupled with ν(C1C5) and ν(C1C2) modes. The $\nu(CF_2)$ mode has a relatively weak intensity and is labeled e. The spectral feature marked f, however, is very intense, and as usual, it involves the C–O stretching motion, in this case specifically the C–O bonds on the end of the monomeric unit, ν(C3O1) and ν(C4O2). Next, the band g is important because it arises from ν^t(C1F1), the stretching motion of the tertiary CF bond, which also contains some ν(C1O1) and ν(C2O2); h is mostly a ν(C1O1) motion but is strongly coupled with ν^t(C1F1). The IR absorption that is used to readily identify PPFPO is the band labeled i; this band, like those assigned to motions that are fingerprints for $(CF_3)_2O$ and $(CF_3CF_2)_2O$, which also occur in the same general spectral region, also involves a motion that is unique to the propylene oxide unit; the mode involves a strongly coupled motion of ν(C1C5), ν(C1C2), $\nu(CF_2)$, and $\nu^s(CF_3)$. Consequently, this mode involves the monomeric unit and may be used for studies requiring this knowledge. Bands at lower frequencies are strongly coupled valence angle bending motions and will be discussed at length in a more detailed analysis for each system.[26] However, we should point out that j, k involve coupled stretching motions of the CF_3 end units; l and m are coupled ν(CO) and ν(CF) motions (and also are the most intense Raman bands); o, p are valence angle bends of the monomeric unit; and q involves the end groups.

Before leaving the PPFPO system, several further comments should be made. First it is straightforward to assign the PPFPO oligomer on the basis of the computed spectrum, that is with the exception of the band labeled e whose intensity is very weak. Second, the spectra of the PPFPO polymeric film also may be reasonably assigned on the same basis; however, in both the oligomer and polymer film we observe some band splitting. Presently we believe this is due to monomers in different conformations, perhaps due to rotations around the C–O bonds.

PPFPO is also synthesized as a copolymer containing $-CF_2O-$ units: the particular PPFPO–PPFF copolymer of interest contains a ratio of propylene oxide to methylene oxide units of $\simeq$20. The infrared spectrum of a thin film of this material is shown in Figure 17 along with the spectrum of PPFPO. Addition of methylene oxide units to the PPFPO systems gives rise to several new absorptions; these are marked by an asterisk in the figure. Figure 18 contains the PPFPO–PPFF spectrum along with the computed spectra of the PPFPO model compound discussed above, and the PPFMO model. As an initial approximation, the additional methylene oxide spectral features are assigned on the basis of the

Table XVII. The Computed Vibrational Frequencies and Intensities for the PPFF Model Compound

vib no.	vib symm	vib freq, cm^{-1}	vib freq scaled (0.89)	computed IR inten, km/mol
33	B	1580.47	1406.62 a'	525.61
32	A	1531.26	1362.82 b'	543.61
31	A	1487.95	1324.28 b'	436.94
30	B	1472.35	1310.39 b'	325.82
29	B	1442.26	1283.61 c'	635.74
28	A	1425.83	1268.99 c'	75.82
27	A	1395.23	1241.76 d'	240.29
26	B	1389.21	1236.40 d'	448.93
25	B	1319.55	1174.40 e'	1235.91
24	A	1080.04	961.23	16.39
23	B	972.55	865.57 f'	50.21
22	A	879.54	782.79	0.64
21	B	831.75	740.25	4.50
20	A	738.10	656.91	1.99
19	B	726.65	646.72 g'	153.63
18	A	721.60	642.23 h'	67.55
17	B	643.66	572.86	10.41
16	A	636.90	566.84	2.71
15	B	576.40	512.99	16.18
14	A	564.33	502.25	3.89
13	A	497.14	442.46	2.06
12	B	475.20	422.93	4.79
11	B	433.95	386.22	2.28
10	A	384.05	341.80	0.25
9	B	371.32	330.47	0.44
8	A	340.70	303.22	0.45
7	A	301.23	268.09	0.06
6	A	168.30	149.79	0.20
5	B	163.24	145.28	0.97
4	B	62.25	55.41	0.03
3	A	45.84	40.80	0.00
2	B	29.34	26.11	0.02
1	A	17.80	15.84	0.01

(26) Pacansky, J. In preparation.

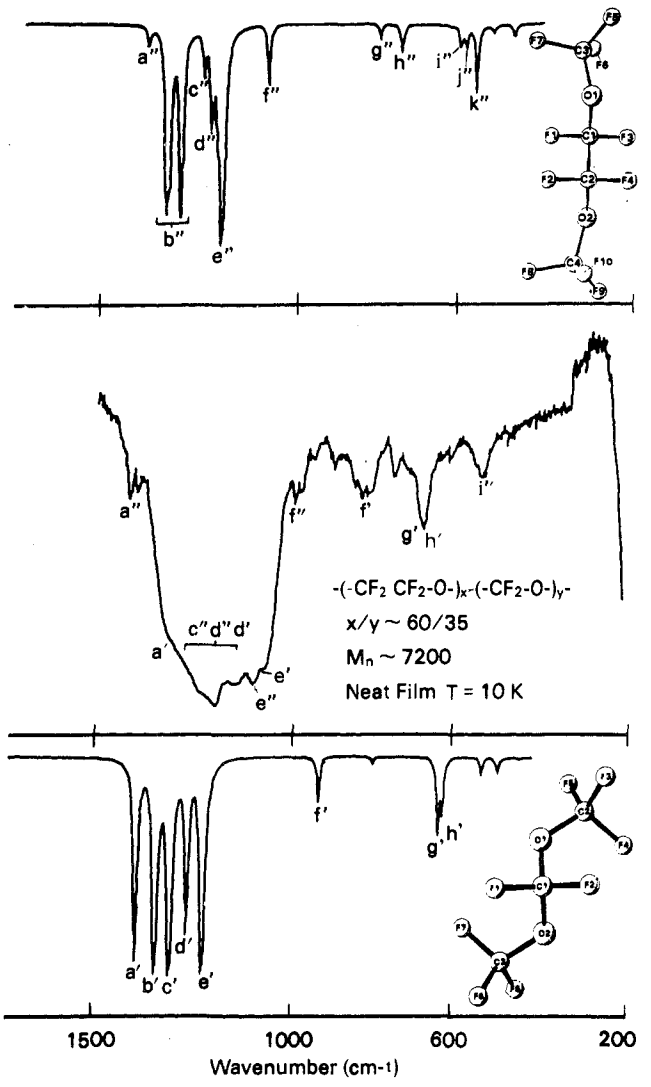

Figure 19. The infrared spectrum of a thin film of PPFFPFEO copolymer $[CF_3CF_2O-(CF_2CF_2O-)_x-(CF_2O)_y-CF_2CF_3]$ and the theoretical spectra of the PPFF and PPFEO model compounds. The copolymer absorptions labeled by a letter have been assigned to particular vibrational motions on the basis of the two model compounds: a'', ν(C1C2); b'', $\nu(CF_3)$; c'', $\nu(CF_2)$; d, $\nu(CF_2) + \nu$(C1O1) + ν(C2O2); e'', ν(C3O1) + ν(C4O2); f'', $\nu(CF_2) + \nu$(C1O1) + ν(C2O2); g'', $\nu(CF_3) + \nu$(C3O1) + ν(C4O2); h'', ν(C1O1) + ν(C2O2) + $\nu(CF_2)$; i'', $\alpha(CF_3)$; j'', $\alpha(CF_3)$; k'', $\alpha(CF_3)$. See Figure 18 for a definition of a'...f' for the PPFF assignments. ν is defined as a bond stretch, and α and β are valence angle bends.

PPFF model spectrum. Table XVII contains a listing of the IR band centers and intensities and lists the bands labeled a' to h'. The assignment of the bands is as follows where the letters used to label the PPFF and PPFPO–PPFF bands are as follows: a' is a coupled stretching of the $\nu(CF_2)$ and $\nu(CF_3)$ groups; b' and c' are attributed to a $\nu(CF_3)$ motion of the end groups; d' is a mixture of $\nu(CF_2)$, ν(C1O1), and ν(C2O2), and hence is a vibrational mode of the monomeric unit; e' has a very strong intensity and is a combination of ν(C1O1), ν(C1O2), ν(C2O1), and ν(C3O2); f' is due to a coupled stretching motion of the terminal C–O bonds and the CF_3 end groups, i.e., ν(C2O1), ν(C1O2) plus $\nu(CF_3)$; g' is assigned to a O1C1O2 valence angle bend, β-(O1C1O2), coupled with valence angle bending of the CF_3 end group $\alpha(CF_3)$; and h' involves $\alpha(CF_2)$ and $\beta(CF_3)$.

The bands labeled a', d', e', and f' in the PPFPO–PPFF spectrum are assigned to $\nu(CF_2)$ and ν(CO) motions on the basis of the assignments discussed in the preceding paragraph. These modes appear to be more characteristic for the formaldehyde unit and hence it is reasonable to expect little perturbations when incorporated into a PPFPO chain.

Table XVIII. The Computed Vibrational Frequencies and Intensities for the PPFEO Model Compound

vib no.	vib symm	vib freq, cm^{-1}	vib freq scaled (0.89)	computed IR inten, km/mol
42	A	1577.75	1404.19 a''	38.19
41	B	1525.54	1357.73 b''	690.28
40	A	1516.58	1349.75 b''	475.95
39	A	1485.07	1321.71 b''	590.77
38	B	1481.99	1318.97 b''	313.77
37	A	1420.59	1264.33 c''	89.68
36	B	1399.15	1245.24 d''	219.31
35	A	1396.29	1242.70 e''	20.39
34	B	1382.87	1230.75 e''	217.60
33	B	1368.10	1217.61 e''	1756.14
32	A	1342.58	1194.90	0.28
31	B	1236.40	1100.40 f''	125.59
30	A	1016.91	905.05	0.38
29	B	922.54	821.06 g''	32.25
28	A	882.78	785.67	0.72
27	B	861.99	767.17 h''	57.61
26	A	731.91	651.40	1.02
25	B	697.26	620.56 i''	30.38
24	A	692.85	616.64 i''	20.82
23	A	678.79	604.12 j''	44.16
22	B	649.98	578.48 k''	148.91
21	B	614.55	546.95	1.14
20	B	602.21	535.97	16.12
19	A	558.08	496.69	0.33
18	B	544.68	484.76	23.03
17	A	535.02	476.16	0.26
16	B	471.57	419.70	0.34
15	A	391.93	348.82	0.25
14	A	387.16	344.57	0.27
13	B	368.78	328.22	3.68
12	A	352.42	313.66	0.06
11	B	333.34	296.67	0.05
10	A	232.55	206.97	4.51
9	B	228.07	202.99	1.40
8	A	223.60	199.00	0.07
7	A	164.04	146.00	0.13
6	B	78.37	69.75	0.32
5	A	71.16	63.34	0.04
4	B	67.96	60.49	0.17
3	A	43.31	38.55	0.00
2	B	37.55	33.42	0.06
1	A	22.35	19.89	0.00

The PPFF–PPFEO copolymer has a ratio of propylene oxide to formaldehyde units of $\simeq$60/35. An IR spectrum of a thin film of the copolymer recorded with the sample temperature at T = 10 K is shown in Figure 19. Note that in comparison to PPFPO and the PPFPO–PPFF copolymer, the spectral region from $\simeq$1500 to 1000 cm^{-1} is very broad, and almost nondescript. In order to at least understand the spectrum, and perhaps assign some of the absorptions in this spectral region, we show the theoretical spectrum of PPFEO at the top of the figure and again the computed spectrum for PPFF at the bottom; the vibrational band centers and intensities for PPFEO are listed in Table XVIII. The labels on the PPFEO calculated spectrum refer to the band assignments given below; those further marked by a prime refer to the PPFF assignment already given in Figure 18; those on the PPFF–PPFEO observed spectrum refer to modes assigned to the copolymer on the basis of the theoretical spectra.

The highest frequency absorption in the calculated spectrum of PPFEO, labeled a'', is the ν(CC) for the only C–C bond in the molecule; like the intensities of the other C–C bonds in the systems already discussed the intensity is at best weak. The modes that follow are $\nu(CF_3)$ modes, labeled b'', from the end groups. The band c'' is primarily a $\nu(CF_2)$ mode while d'' is a mixture of $\nu(CF_2)$, ν(C1O1), and ν(C2O2). The most intense band in the spectrum, e'', is the stretching frequency of the C–O bonds, ν-(C3O1) and ν(C4O2). The bands f'', g'', and h'' are due to motions formed by coupled stretching vibrations of a large number of bonds; f'' arises from $\nu(CF_2)$, ν(C1O1), and ν(C2O2); g'' is a mixture of $\nu(CF_3)$, ν(C3O1), and ν(C4O2); and h'' contains

ν(C1O1), ν(C2O2), and $\nu(CF_2)$ motions. The band i'' is a valence angle bending motion in the CF_3 end groups, $\alpha(CF_3)$.

The absorptions in the observed copolymer spectrum are assigned as follows: the C–C stretching frequency in the PPFEO calculated spectrum has the highest frequency and also one of weakest intensities; therefore, the weak features marked a'' are assigned to the ν(CC) modes in the propylene oxide unit of the copolymer. Somewhat lower in frequency but of stronger intensity is the CF stretching mode of the CF_2 unit in PPFF; the unresolved but detectable feature marked a' is thus assigned to the $\nu(CF_2)$ of the $-CF_2-O-$ monomeric unit. The broad feature branded c'', d'', and d' is most likely a convolution of the stretches from the CF_2 units in the propylene oxide group and bands due to coupled motions of stretching modes in the CF_2 and C–O groups in both the formaldehyde and propylene oxide monomeric units. The bands marked e'' and e' are both due to C–O stretches which are very intense; e'' has a higher frequency and is assigned to the ν(CO) in CF_2–O while the lower frequency band is assigned to the propylene oxide unit. The absorptions, referred to as f'' and f', are most likely motions due to coupled stretches within the propylene oxide and formaldehyde monomeric units, respectively. Those are the lower frequencies assigned to valence angle bending motions; g' and h' are assigned to the formaldehyde unit while i'' is assigned to the propylene unit.

Registry No. PPFEO (homopolymer), 26591-06-0; PPFEO (SRU), 32107-75-8; PPFPO (homopolymer), 25038-02-2; PPFPO (homopolymer), 35038-02-2; PPFPO (SRU), 62253-59-2: CF_3OCF_3, 1479-49-8; $CF_3CF_2OCF_2CF_3$, 358-21-4; $CF_3CF_2OCF_3$, 665-16-7; $CF_2(OCF_3)_2$, 53772-78-4; $CF_3O(CF_2)_2OCF_3$, 378-11-0; $CF_3OCF(CF_3)CF_2OCF_3$, 95842-02-7.

Carbon Dioxide Activation by Cobalt(I) Macrocycles: Factors Affecting CO_2 and CO Binding

Etsuko Fujita,* Carol Creutz,* Norman Sutin, and David J. Szalda[1]

Contribution from the Chemistry Department, Brookhaven National Laboratory, Upton, New York 11973. *Received April 26, 1990*

Abstract: The cobalt(I) complexes of several 14-membered tetraazamacrocycles were prepared in CH_3CN by either electrochemical or sodium amalgam reduction. The electronic absorption spectra and other physical properties of the Co^I, Co^I–CO_2 and Co^I–CO complexes are reported. The CO_2 and CO binding constants were determined by spectroscopic and/or electrochemical methods. The binding constants range from 5×10^4 to $\geq 3 \times 10^8$ M^{-1} for CO and from ≤ 0.5 to $> 10^6$ M^{-1} for CO_2 at 25 °C. Both binding constants increase as the $CoL^{2+/+}$ reduction potentials (which range from −0.34 to −1.65 V vs SCE in CH_3CN) become more negative. Thus charge transfer from Co^I to CO_2 or CO is an important factor in stabilizing these adducts. However, hydrogen-bonding interactions between the bound CO_2 and amine macrocycle N–H protons may serve to additionally stabilize the adduct in some cases, while steric repulsion by the macrocycle methyl groups may destabilize the adducts, depending upon the complex. The equilibrium ratios of N-meso and N-rac isomers of (5,7,7,12,14,14-hexamethyl-1,4,8,11-tetraazacyclotetradeca-4,11-diene cobalt(I) and -(II) complexes were determined by ^1H NMR; the N-rac isomers of both predominate in CD_3CN at room temperature. The crystal and molecular structure of the perchlorate salt of (3,5,7,7,10,12,14,14-octamethyl-1,4,8,11-tetraazacyclotetradeca-4,11-diene cobalt(I) was determined from single-crystal X-ray diffraction data collected with use of Mo Kα radiation. Crystallographic data: space group $P\bar{1}$ with $a = 8.433$ (2) Å, $b = 18.333$ (4) Å, $c = 7.257$ (2) Å, $\alpha = 100.22$ (2)°, $\beta = 91.29$ (2)°, $\gamma = 87.68$ (2)°, $V = 1103$ (1) Å^3, $Z = 2$ ($R = 0.085$, $R_w = 0.105$). The two square-planar cobalt atoms in the asymmetric unit are situated on crystallographic inversion centers.

Introduction

Although there has been intense interest[2-6] in the electrochemical and photochemical activation of carbon dioxide promoted by transition-metal complexes, only a few detailed mechanistic studies of CO_2 binding to metal complexes have been published. Since Curtis' template synthesis of the $Ni^{II}L_5^{2+}$ (L_5 = 5,7,7,12,14,14-hexamethyl-1,4,8,11-tetraazacyclotetradeca-4,11-diene) complex,[7] many 14-membered tetraazamacrocyclic complexes have shown interesting properties, especially as catalysts for H_2O[8] and CO_2[9,10] reduction. Fisher and Eisenberg[9] reported the electrocatalytic activity of the cobalt(II) and nickel(II) macrocycles in CO_2 reduction in acetonitrile–water mixtures. Gangi and Durand[11] used differential pulse polarography to characterize the reversible binding of CO_2 to $Co^IL_5^+$ ($K_{CO_2} = 7 \times 10^4$ M^{-1}) in dimethyl sulfoxide. We have investigated the reversible binding of CO_2, CO, and H^+ to *N-rac*-$Co^IL_5^+$ in H_2O[12] and CH_3CN,[10,12c] and reversible binding of CO_2 to a series of cobalt(I) macrocycles in DMSO has recently been reported.[13] We have also studied a CO_2 reduction pathway involving two cobalt

(1) Permanent address: Department of Natural Sciences, Baruch College, Manhattan, NY 10010.

(2) Recent reviews: (a) Creutz, C. In *Electrochemical and Electrocatalytic Reduction of Carbon Dioxide*; Sullivan, B. P., Ed.; Elsevier: Amsterdam, in press. (b) Walther, D. *Coord. Chem. Rev.* **1987**, *79*, 135. (c) Ayers, W. M., Ed. *Catalytic Activation of Carbon Dioxide*; ACS Symp. Ser.; American Chemical Society: Washington, D.C., 1988. (d) Behr, A. *Carbon Dioxide Activation by Metal Complexes*; VCH: Weinheim, 1988. (e) Braunstein, D.; Matt, D.; Nobel, D. *Chem. Rev.* **1988**, *88*, 747. (f) Kolomnikov, I. S.; Lysak, T. V.; Rusakov, S. L.; Kharitonov, Y. Y. *Russ. Chem. Rev.* **1988**, *57*, 406. (g) Behr, A. *Angew. Chem., Int. Engl. Ed.* **1988**, *27*, 661. (h) Collin, J. P.; Sauvage, J. P. *Coord. Chem. Rev.* **1989**, *93*, 245.

(3) Recent studies of CO_2 electrochemical reduction promoted by transition-metal complexes: (a) Bruce, M. R. M.; Megehee, E.; Sullivan, B. P.; Thorp, H.; O'Toole, T. R.; Downard, A.; Meyer, T. J. *Organometallics* **1988**, *7*, 238. (b) Bolinger, C. M.; Story, N.; Sullivan, B. P.; Meyer, T. J. *Inorg. Chem.* **1988**, *27*, 4582. (c) Ishida, H.; Tanaka, K.; Tanaka, T. *Chem. Lett.* **1988**, 339. (d) Grunewald, G.; Drago, R. S. *J. Chem. Soc., Chem. Commun.* **1988**, 1206. (e) Kim, J. J.; Summers, D. P.; Frese, K. W. *J. Electroanal. Chem.* **1988**, *245*, 223. (f) Corrigan, D.; Weaver, M. J. *J. Electroanal. Chem.* **1988**, *241*, 143. (g) Hammouche, M.; Lexa, D.; Savéant, J. M.; Momenteau, M. *J. Electroanal. Chem.* **1988**, *249*, 347. (h) Tanaka, K.; Miyamoto, H.; Tanaka, T. *Chem. Lett.* **1988**, 2033. (i) Frese, K. W.; Summers, D. P.; Cinibulk, M. *J. Electrochem. Soc.* **1988**, *135*, 264. (j) Arai, G.; Harashina, T.; Yasumori, I. *Chem. Lett.* **1989**, 1215. (k) Tanaka, K.; Matsui, T.; Tanaka, T. *J. Am. Chem. Soc.* **1989**, *111*, 3765. (l) Azuma, M.; Hashimoto, K.; Hiramoto, M.; Watanabe, M.; Sakata, T. *J. Electroanal. Chem.* **1989**, *260*, 441. (m) Sugiura, K.; Kuwabata, S.; Yoneyama, H. *J. Am. Chem. Soc.* **1989**, *111*, 2361. (n) Garnier, L.; Rollin, Y.; Périchon, J. *New J. Chem.* **1989**, *13*, 53.

0002-7863/91/1513-343$02.50/0